

1962

A Study of Luminous-Shock Fronts in an Electromagnetic Shock Tube

James Franklin Roach
College of William & Mary - Arts & Sciences

Follow this and additional works at: <https://scholarworks.wm.edu/etd>



Part of the [Electromagnetics and Photonics Commons](#)

Recommended Citation

Roach, James Franklin, "A Study of Luminous-Shock Fronts in an Electromagnetic Shock Tube" (1962). *Dissertations, Theses, and Masters Projects*. Paper 1539624535.
<https://dx.doi.org/doi:10.21220/s2-tg9r-4y67>

This Thesis is brought to you for free and open access by the Theses, Dissertations, & Master Projects at W&M ScholarWorks. It has been accepted for inclusion in Dissertations, Theses, and Masters Projects by an authorized administrator of W&M ScholarWorks. For more information, please contact scholarworks@wm.edu.

**A STUDY OF LUMINOUS-SHOCK FRONTS IN
// AN ELECTROMAGNETIC SHOCK TUBE**

A Thesis

Presented to

**The Faculty of the Department of Physics
The College of William and Mary in Virginia**

In Partial Fulfillment

**Of the Requirements for the Degree of
Master of Arts**

By

James Franklin Roach

August 1962

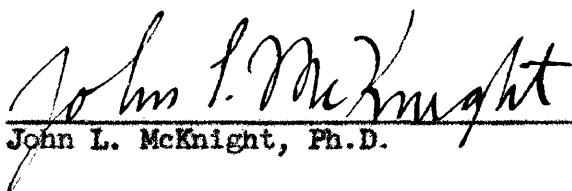
APPROVAL SHEET

This thesis is submitted in partial fulfillment of
the requirements for the degree of
Master of Arts




Author


Approved, August 1962:



John L. McKnight, Ph.D.



Melvin A. Pittman, Ph.D.



Donald E. McLennan, Ph.D.

ACKNOWLEDGMENTS

The writer is indebted to Dr. Wayne D. Erickson under whose supervision this research was carried out. The author expresses his appreciation to Dr. John L. McKnight for his criticism and guidance in preparation of the text. He is grateful to Mr. Joseph A. Poslik who collaborated in the electrical design of the experimental apparatus. The author thanks Mrs. Christine B. Richie, who aided in the data analysis and Mrs. Barbara B. Holley, who helped prepare the figures. He wishes also to acknowledge the use of the facilities at the Langley Research Center, where the research was undertaken.

TABLE OF CONTENTS

| | Page |
|---|------|
| ACKNOWLEDGMENTS | iii |
| LIST OF FIGURES | v |
| ABSTRACT | vii |
| INTRODUCTION | 2 |
| Chapter | |
| I. DESCRIPTION OF FACILITY | 6 |
| A. Shock Tube | 6 |
| B. Electrical Circuit | 9 |
| C. Air Gap Switch | 11 |
| D. Diagnostic Techniques | 13 |
| II. RESULTS AND ANALYSIS | 14 |
| A. General Comments | 14 |
| B. Electrical Characteristics | 17 |
| C. Pinched Discharge | 21 |
| D. Performance of Shock Generators | 23 |
| E. Shock Profile | 35 |
| F. Reflected Luminous Fronts | 37 |
| G. Time-Integrated Spectra | 43 |
| III. SUMMARY AND CONCLUDING REMARKS | 48 |
| REFERENCES | 52 |

LIST OF FIGURES

| Figure | Page |
|---|------|
| 1. Photograph of facility | 7 |
| 2. Schematic of electromagnetic shock tube | 8 |
| 3. Circuit diagram | 10 |
| 4. Rogowski electrode configuration atmospheric switch . . | 12 |
| 5. Sketch of electrode configurations | 16 |
| 6. Equivalent circuit | 18 |
| 7. Typical scope trace of voltage output from field coil and calculated circuit parameters | 20 |
| 8. Characteristics of pinch discharge | 22 |
| 9. Luminous-front velocity as a function of initial pressure for button-ring configuration | 25 |
| 10. Luminous-front velocity as a function of initial pressure for spindle-cone configuration | 26 |
| 11. Luminous-front velocity as a function of initial pressure for the pinch-tube configuration | 27 |
| 12. Time separation of secondary waves generated by button-ring configuration | 29 |
| 13. Typical velocity smears showing luminous-front attenuation and multiple-shock interaction | 30 |
| 14. Attenuation of luminous front generated by pinch- tube configuration | 31 |
| 15. Interaction of primary luminous front and secondary wave | 32 |

| Figure | Page |
|---|------|
| 16. Time-average photographs of luminous bow waves | 34 |
| 17. Profile of shocks generated by pinch tube | 36 |
| 18. Velocity smears of reflection off brass plug | 38 |
| 19. Time-average photographs of hot gas reflecting off brass plug | 39 |
| 20. Average effect of incident shock velocity on reflected shock velocity at plug | 41 |
| 21. Average effect of initial pressure on ratio of reflected shock velocity at plug | 42 |
| 22. Average effect of incident shock velocity on reflected shock velocity at 10.2 cm from plug | 44 |
| 23. Time-integrated spectra of discharge from pinch tube . . . | 45 |
| 24. Time-integrated spectra of air gap switch discharge . . . | 47 |

ABSTRACT

A study is made of strong luminous-shock fronts which are generated in a pulsed linear discharge tube. A high-voltage, low-inductance capacitor bank supplies driving energies up to 3,125 joules. Strong shock waves (shock Mach numbers, $M_s = 20$ to 150) are propagated into ambient air at initial pressures of 10 to 1,000 microns of mercury. The primary and reflected luminous-shock fronts are examined with a rotating mirror camera and time-average photography. The primary waves show strong attenuation and are complicated by interactions with secondary fronts. The measured reflected velocities are found to be greater than expected on the basis of equilibrium real-air theory. Time-integrated spectra of the discharge in the spectral region 3,500 to 5,000 Å are characteristic of spark spectra in a low-pressure air discharge. The investigation points out the nonuniformity and the turbulent nature of the short-duration (tens of microseconds) shock flow. It is concluded, therefore, that the use of such flows for studies in hypersonic aerodynamics must be approached with reservation.

A STUDY OF LUMINOUS-SHOCK FRONTS IN
AN ELECTROMAGNETIC SHOCK TUBE

INTRODUCTION

In the conventional one-dimensional pressure-driven shock tube (ref. 1) a diaphragm separates two volumes of gas at different pressures. When the diaphragm is removed, a compression wave propagates into the low-pressure chamber and an expansion wave propagates into the high-pressure chamber. In the case of a high-pressure ratio the compression wave steepens into a shock front. The shock front is an amplitude-dependent disturbance through which a change of entropy occurs. It propagates at supersonic speed relative to the acoustic speed in the low-pressure chamber. The strength of the shock is proportional to the pressure ratio and the speed-of-sound ratio of the driver (high-pressure gas) to the driven gas. This can be accomplished in a variety of ways. The driver gas can be heated by an electric discharge or a combustion process increasing both the pressure and speed-of-sound ratio across the diaphragm. The speed-of-sound ratio can be maximized by selecting low molecular weight driver gases such as hydrogen and helium. Further methods are the application of multiple-diaphragm techniques and the use of varying cross-section channels. A survey of techniques and theory of the shock tube in its many forms is found in reference 2. In all the cases mentioned diaphragms must be selected which can survive the high-pressure ratio and have an efficient bursting process. This mechanical requirement has, for the present, limited the diaphragm shock tube to shock Mach numbers (the ratio of the shock front velocity to the speed of sound in the unshocked gas) of less than $M_s = 30$, as, for example, in the electrically

driven shock tubes (refs. 3 and 4). An alternative method for producing strong shocks without the necessity of a diaphragm is the rapid release of a large amount of energy creating a local high temperature and pressure. The expansion of the gas generates a strong, attenuating shock wave. This is the familiar process occurring in explosions or blast waves (ref. 5). A spark discharge tube can be used to produce very strong shocks in much the same way. The development of the spark discharge tube and the progress of other electromagnetic devices for generating shock waves are outlined in the following paragraph.

In 1951 Fowler and Lee (ref. 6) pointed out that the luminosity appearing in the appendages off a main electrical discharge (the so-called Rayleigh afterglow), was "highly concentrated in a series of advancing fronts, rather than ejected as a tongue or jet." In a later paper by Fowler et al. (ref. 7) the nature of these luminous waves was examined in a T-tube discharge. Their results suggested the kinship of these waves with shock waves and large-amplitude acoustical disturbances. In general, the luminous-front velocity was directly proportional to the capacitor energy and inversely proportional to the initial pressure and molecular weight of the test gas. The attenuation of the disturbance as well as "echo" or reflected waves were observed. Fowler et al. (ref. 8) pointed out that at low densities the strongly self-luminous shock front was the principal manifestation of the hot-gas expansion. Saha temperature excitation processes were expected to be important in explaining these waves. Since the shocked gases were shown to be highly ionized it was suggested that the application of external magnetic fields would increase the driving force, which previously was derived mainly from Joule heating. Kolb (ref. 9) and Kash (ref. 10) modified the T-tube shock generator to include

several field coil and "backstrap" geometries to obtain a Lorentz volume force on the ionized gases. They were able to increase greatly the energy transfer to the gas and thus obtained much stronger shocks. Josephson (ref. 11) introduced the linear "tapered tube" discharge for generating strong axial shocks. In this case the current discharge takes place along the axis of the shock tube and a strong "pinching" by the self-induced magnetic field is the major driving force. Typically shock Mach numbers on the order of $M_s = 150$ in deuterium and $M_s = 50$ in air are readily attainable. Other types of electromagnetic shock tubes have been reported in the literature and a good summary is found in a report by Ziemer (ref. 12).

Such devices have a potential for many investigations dealing with extreme temperature gases and hypersonic flows. The investigation reported in this thesis arose from the possibility of using an electromagnetic shock tube to study the problem of radiation heat transfer to the nose of a reentry vehicle. Ziemer (ref. 13) successfully investigated the effect of a magnetic field on the shock standoff distance and stagnation point heat transfer on a hemispherical model using the flow in a tapered-tube electromagnetic shock tube operated in air. The development of a thin-film heat-transfer gauge (ref. 14) used in his investigation indicates some of the difficulties in instrumentation of such short-duration flows (on the order of tens of microseconds). For radiation studies these times would be sufficient, but a closer study of the flow and contamination was necessary since radiation levels can be greatly affected by nonequilibrium processes and contamination. The writer visited Dr. Ziemer in July 1960 to discuss plans to develop an electromagnetic shock tube at Langley Research Center. By September 1960 a 7.5 KV, 386

tapered-tube device had been constructed with existing equipment. Although strong luminous fronts were generated, the contamination from electrode erosion was severe due to the long ringing period of the discharge. Subsequently, plans for a high-voltage, low-inductance capacitor system were initiated. The new facility was first operated in September 1961. This thesis presents a description of the latter electromagnetic shock tube and the results of studies made on the luminous fronts to determine the suitability of the shock flow for studying the radiant heating problem to reentry vehicles.

CHAPTER I

DESCRIPTION OF FACILITY

A. Shock Tube

The shock tube used in this investigation is similar to the tapered-tube-type device described by Ziemer (ref. 13). A photograph of the shock tube and associated electrical equipment is presented in figure 1 and the major components are pointed out. Figure 2 is a schematic of the facility. The shock tube proper is a 3-inch inner-diameter, double-tough Pyrex glass pipe. Several pipe lengths from 18 inches to 48 inches were used. Standard glass fittings join the shock tube to the discharge region and the end plate. The tapered discharge region was obtained from Grenier Glass Blowing Laboratories, Los Angeles, California. It has a parabolic contour which tapers from 3 inches at the exit of the discharge region to $3/4$ inch at the position of the button electrode. A 1-inch precision-bore tubing allows for an O-ring vacuum seal. O-rings are also used at the ends of the uniform glass pipe section. The shock tube is evacuated to initial pressures between 10 and 1,000 microns of mercury by a Welch Duo-Seal mechanical pump. A 0 to 1,000-micron Hastings gauge measured the initial pressure. The pressure was controlled by a Teflon-seat bleed valve. Ambient room air was the testing medium. An observation port with schlieren quality windows $2\frac{1}{2}$ inches in diameter is presently being used in an effort to obtain schlieren pictures of the standing waves on blunt bodies

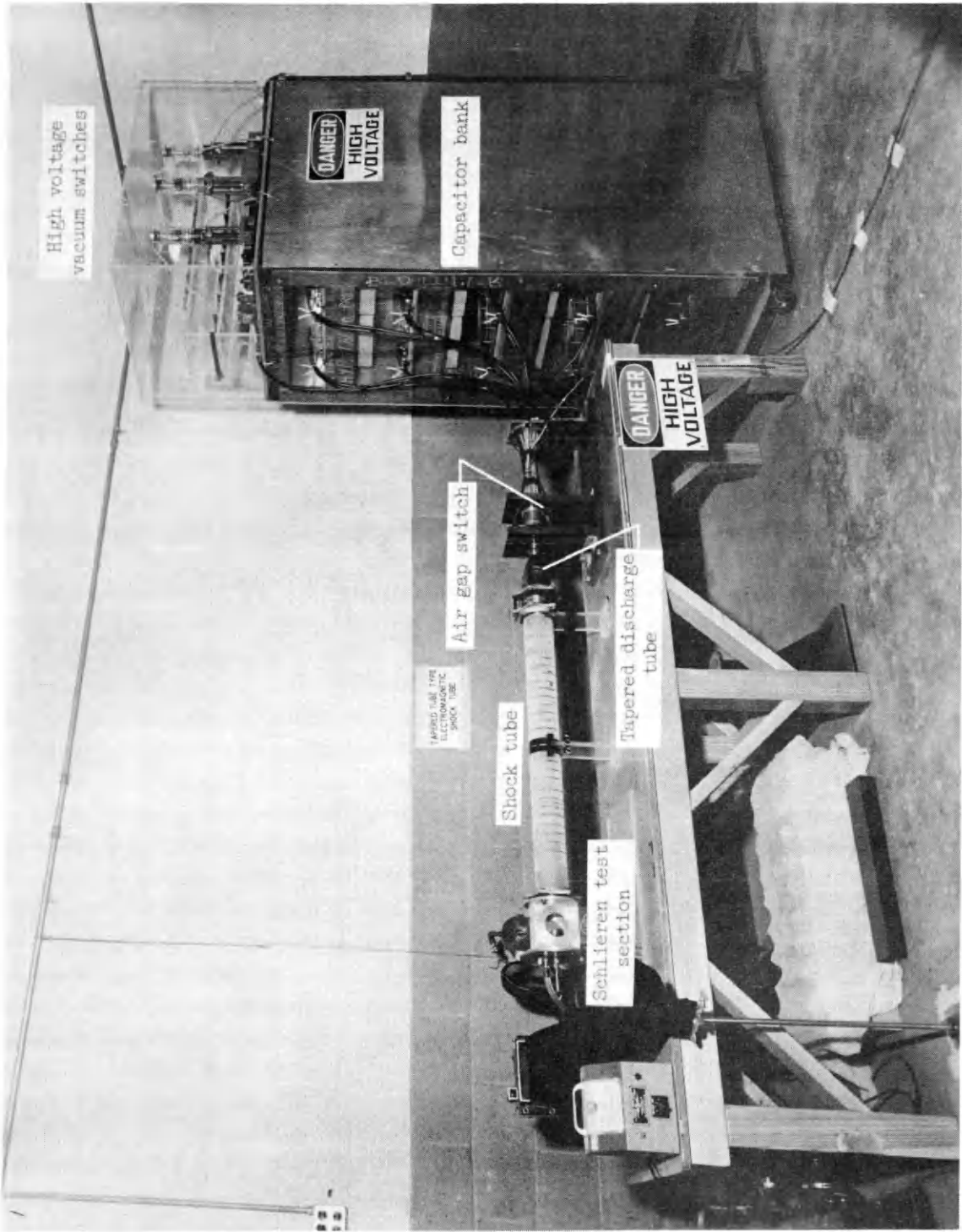


Figure 1.- Tapered tube electromagnetic shock tube.

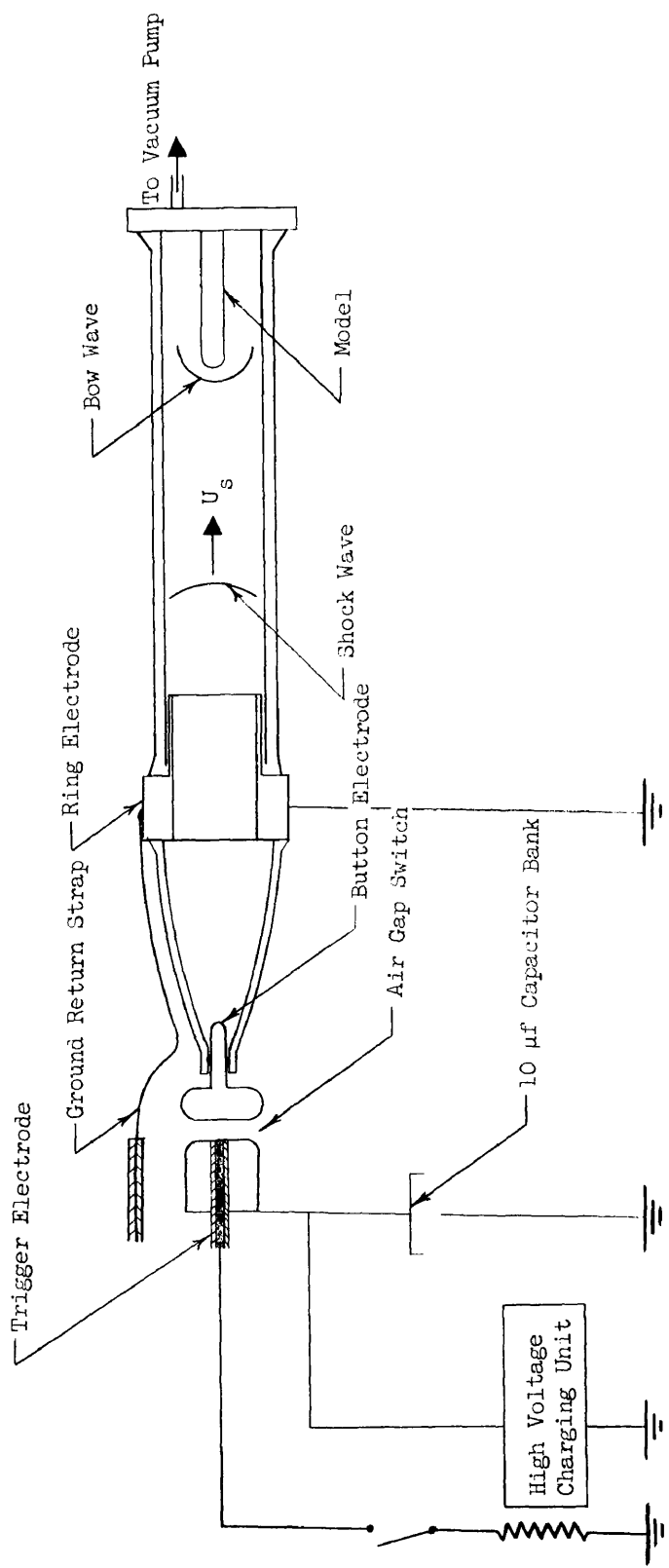


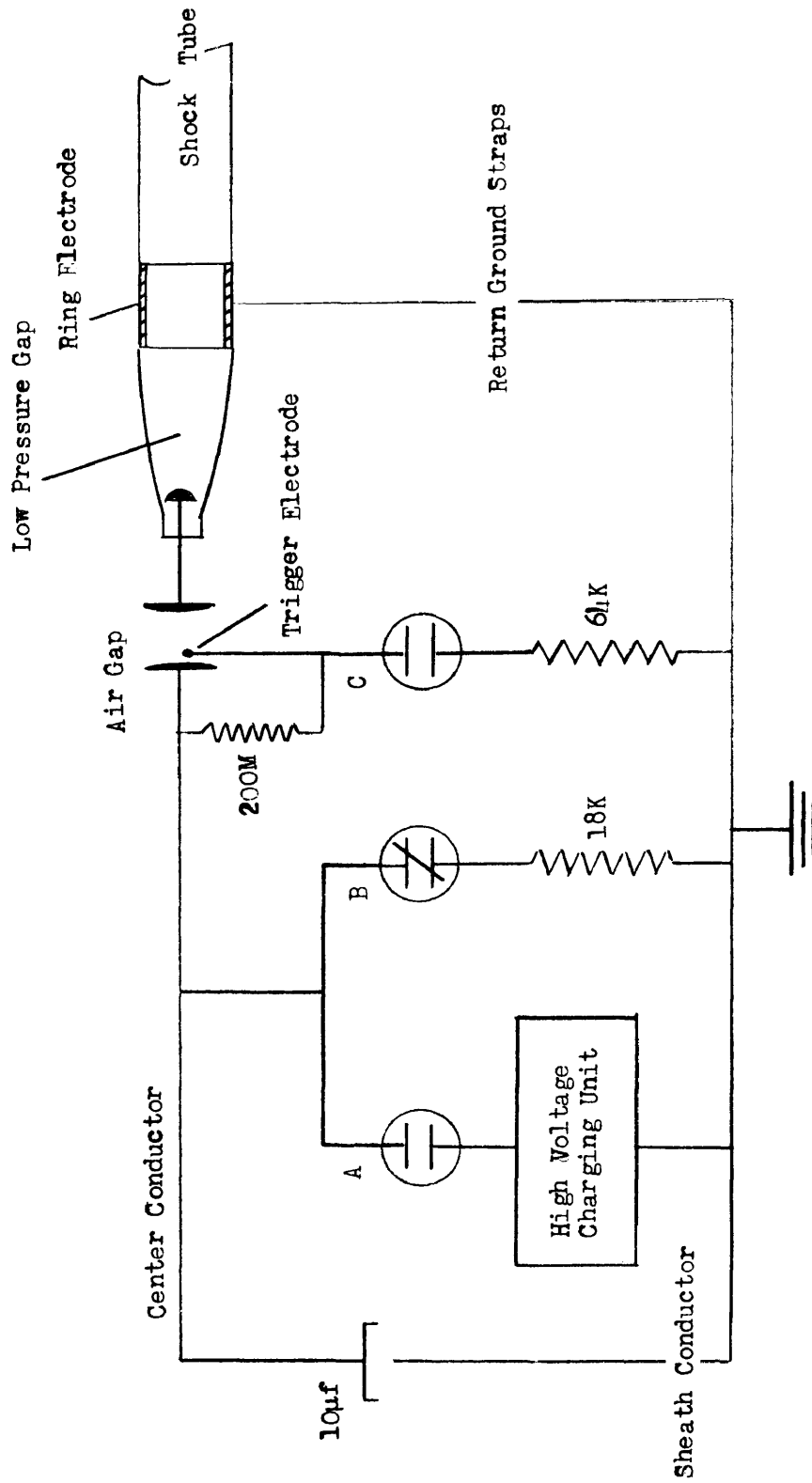
Figure 2.- Schematic of electromagnetic shock tube.

in the shock flow. This work is in a preliminary stage and is not reported in this thesis.

B. Electrical Circuit

The electrical system consists of a bank of 10 one-microfarad low-inductance capacitors connected in parallel. The capacitors were purchased from Axel Electronics Corporation and are rated at 30 KV with a ringing frequency of 150 KC. RG/8-U coax cable connects the capacitors to the discharge tube. In order to minimize the inductance two cables were used for each capacitor. The sheaths are terminated by a press fit between two brass pieces. The center conductors extend for 10 inches and are then terminated at the rear of the positive air gap switch electrode by means of lugs. A second copper electrode completes the air gap switch and extends into the low-pressure discharge tube and is referred to as the button electrode. A copper ring $2\frac{1}{2}$ inches in length serves as the negative electrode in the discharge tube. The circuit is completed by six copper straps, $\frac{1}{4}$ inch by $\frac{1}{32}$ inch, which are laid along the tapered glass section. The straps are then insulated and pass over the air gap switch and center conductor bundle to the sheath termination point.

Figure 3 shows a circuit diagram of the facility. The charging, firing, and shorting phases of the operation are controlled by three Jennings High Voltage Vacuum Relay switches. These switches are solenoid operated at 115 volts a-c by a remote-control panel (not shown) which is isolated from the high voltage. The charging and firing switches are normally open and the shorting switch is normally closed. The capacitors are charged by a NJE Corporation 30-KV, 10-ma power supply which is



- A HV Vacuum Charging Switch
- B Shorting Switch
- C Triggering Switch

Figure 3.- Circuit diagram.

manually operated. A 200-megohm bank of carbon resistors maintains the brass trigger rod and the positive air gap electrode at the same potential during the charging cycle. This was found necessary because the vacuum switch had enough leakage current to trigger the air gap before the required charging voltage was obtained. The shorting and firing resistors are banks of 3-K, 160-watt and 5-K, 50-watt Electrohm resistors, respectively. All grounds are terminated to the capacitor rack which is grounded appropriately to the building.

C. Air Gap Switch

The switch is shown in figure 4. The surfaces of the electrodes are approximate equipotentials of a parallel plate capacitor for a gap separation of 0.37 inch. This distance, as determined from the Paschen curve for air, will hold off 30 KV at S. T. P. The analysis of this electrode configuration is attributed to Rogowski (ref. 15) who calculated the equipotentials at the edge of a parallel plate capacitor. In the parallel portions of the electrodes the field strength is 100 percent and drops off rapidly along the rounded edges. A rubber insulated brass rod inserted along the axis of the positive electrode is maintained at the same potential as the positive electrode by the 200M resistor. When switch A is closed the brass rod is grounded through the 64K resistor bank. The 200M resistance is shunted by the air dielectric and current is drawn from the positive electrode to the brass trigger. Sufficient ionization is present to initiate complete breakdown of the atmospheric gap and consequently of the low-pressure gap. Negligible current is then drawn by the firing resistor. The switch has performed reliably throughout the investigation;

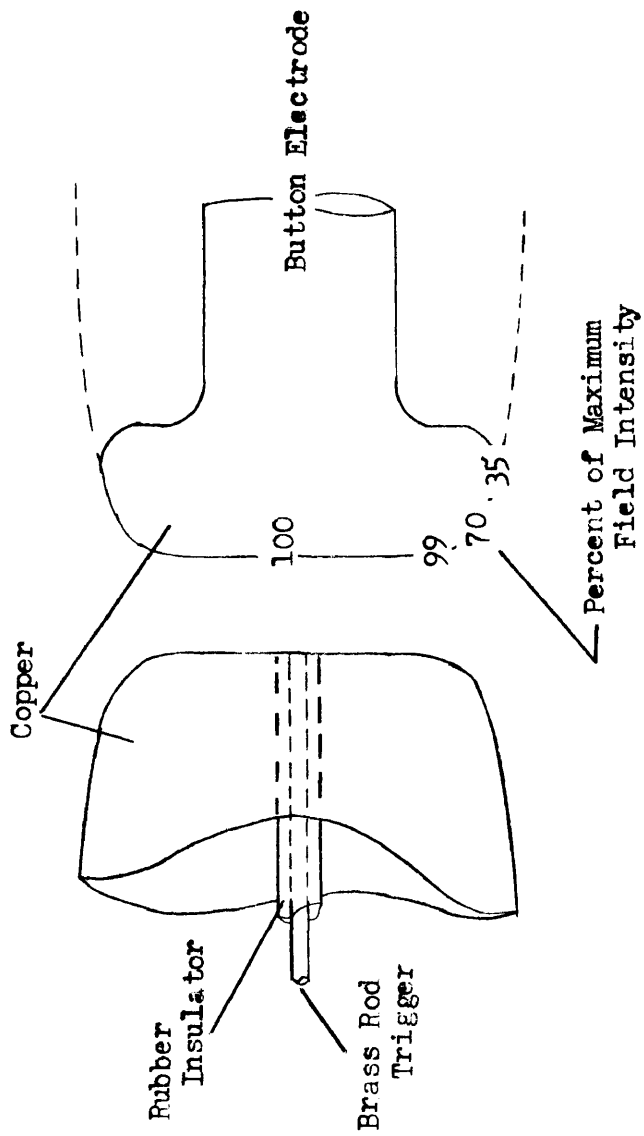


Figure 4.- Rogowski electrode configuration atmospheric switch (scale 1:1).

the discharge always occurs in the center portion of the gap in a diameter of about 1 inch as determined by the eroded area on the electrode surfaces.

D. Diagnostic Techniques

The luminous fronts were analyzed mainly by a rotating mirror camera. A Beckman-Whitley Model 193-5 camera with writing speeds up to 3 mm/microsecond using an air drive was employed. The smear pictures were obtained on black and white 35-mm Kodak Tri-X Pan strip film. Time-average photographs of the lumination provided qualitative information of the shock-tube behavior. A 1/10-microsecond Kerr cell was used for a limited time period in the study of the pinch discharge mechanism. A 545-A Textronix scope and a several-turn field coil placed near the discharge region supplied information about the effective circuit characteristics. Time-integrated spectra were obtained with a Cenco grating spectrograph. The dispersion is roughly $16 \text{ \AA}/\text{mm}$ and allows spectra to be taken in the first order between 2,350 and 7,000 \AA . A concave grating of the replica type having 15,000 lines per inch and a focal length of 55 cm was employed. Certain portions of the grating surface were masked to minimize "ghosts" appearing in calibration spectra due to the grating imperfections.

CHAPTER II

RESULTS AND ANALYSIS

A. General Remarks

In operating the shock tube the capacitor bank is charged to voltages between 12.5 and 22 KV. The discharge is initiated by triggering the air gap switch. A fraction of the total energy stored by the capacitors is then added to the low-pressure gas. The energy available for generating the shock waves can be expressed as the sum of two terms:

$$\frac{\vec{B}^2}{8\pi\rho} + (\beta - 1)\frac{p}{\rho}$$

p/ρ

driver gas pressure per unit mass

β

enthalpy parameter; for a perfect gas is $\gamma/\gamma - 1$,

where γ is the ratio of specific heats

\vec{B}

magnetic field vector

The first term is the energy per unit mass in the magnetic field. Since the gas is highly ionized by the electric discharge, this field applies a volume driving force $\vec{F}_v = \vec{J} \times \vec{B}$ to the gas, where \vec{J} is the current density. The second energy term expresses the increase in the internal energy of the gas and is derived from the Joule heating, $\vec{J}^2 R$, where R is the resistance of the conducting gas. The magnetic field is linearly dependent on the current and therefore both energy terms are proportional to the square of the discharge current. The shock velocity is also

dependent upon the initial rate of current rise with time. For a constant L-C circuit the maximum current and derivative at time zero are:

$$i_{\max} = V_c \sqrt{\frac{C}{L}}$$

$$\left(\frac{di}{dt}\right)_{t=0} = \frac{V_c}{L}$$

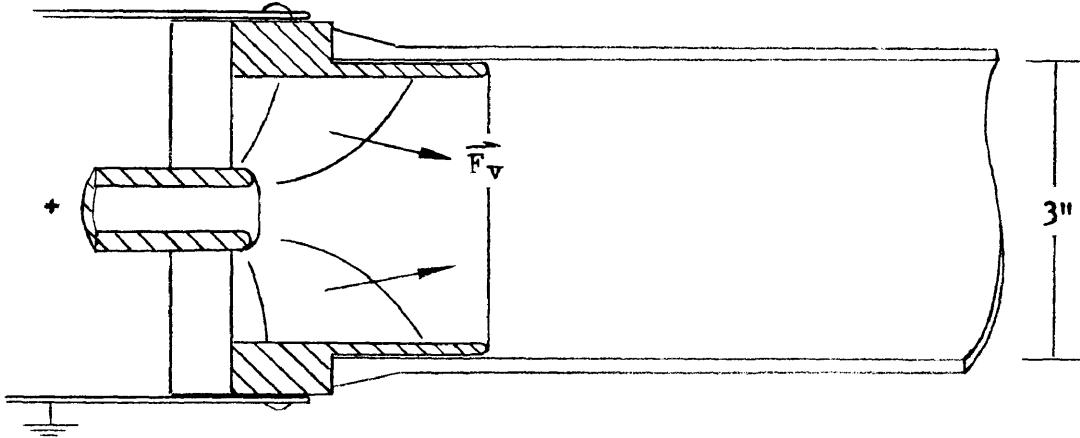
V_c initial charge on the capacitor

C total system capacitance

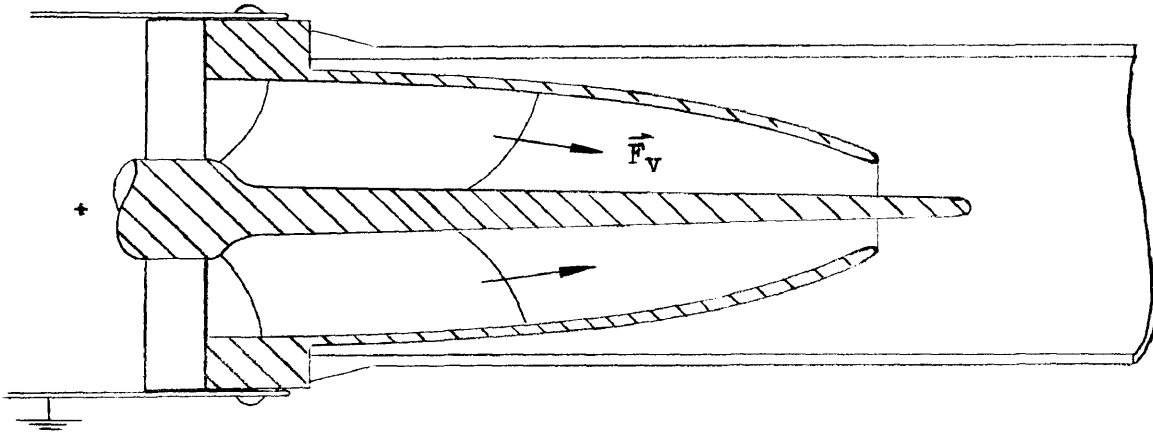
L total system inductance

Consequently, to obtain good energy transfer to the gas a high-voltage and low-inductance system is necessary. Josephson and Hales (ref. 16) give a more complete analysis of design criteria for producing strong shocks with a tapered-tube electromagnetic shock tube.

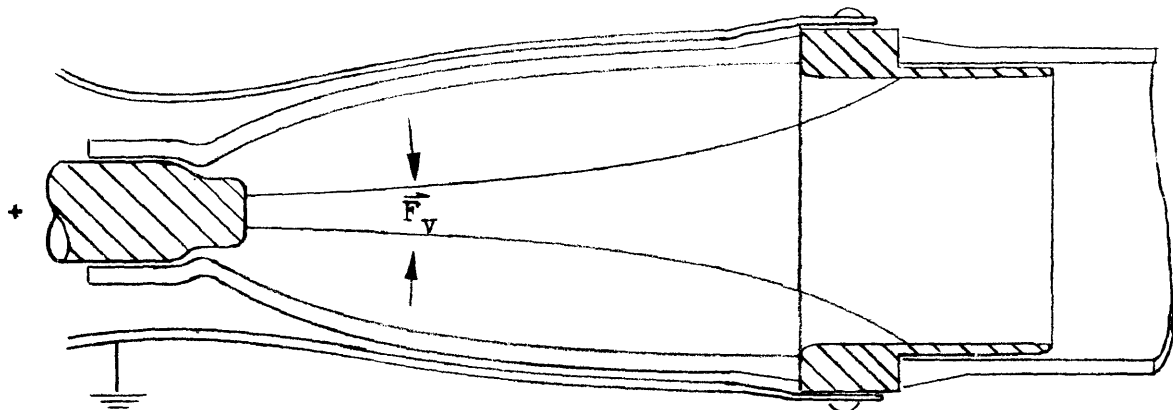
Besides the pinch-tube electrode configuration, two other configurations were investigated. They are sketched in figure 5. The general direction of the Lorentz driving force, F_v , is indicated for each configuration. In the hollow button-ring and spindle-cone configurations the current paths are inclined at a steep angle to the shock axis and the magnetic driving force acts in the direction of the shock flow; in the pinch tube the current is in the direction of the axis and thus the conducting gas is driven towards the center of the tube. The luminous fronts produced by these generators are examined with the rotating mirror camera and time-average photography in order to determine the characteristics of the shock flow. The primary waves, shock profiles, and reflected waves are discussed in sections D, E, and F. The time-integrated



(a) Hollow button-ring electrode configuration.



(b) Aluminum spindle-cone electrode configuration.



(c) Pinch tube electrode configuration.

Figure 5.- Sketch of electrode configurations (scale 1:2).

spéctra are then presented in section G. Before proceeding to the flow analysis, the electrical characteristics of the ringing discharge and the mechanism of the pinch phenomena will be discussed in the following two sections.

B. Electrical Characteristics

The shock-tube circuit can be analyzed on the basis of the equivalent circuit shown in figure 6. V_c is the initial charge on the capacitor bank. The external inductance and resistance are L_e and R_e and are essentially constant. The major contributor to L_e is the air gap switch. The inductance and resistance of the load or discharge tube are given by L_L and R_L and are variables in time. The instantaneous voltage across the capacitor bank is then given by:

$$V = i(R_e + R_L) + \frac{d}{dt} i(L_e + L_L)$$

$$= \left\{ iR_e + L_e \frac{di}{dt} \right\} + \left\{ i \left(R_L + \frac{dL_L}{dt} \right) + L_L \frac{di}{dt} \right\}$$

If the current is observed over several cycles, then the first term, which is the voltage across the external inductance and resistance, is predominant and the circuit is treated as a damped L-R-C discharge. The second term, which is the voltage at the button electrode, is important in determining the driving characteristics of the generator, but for the purpose of finding the effective resistance and inductance of the circuit it can be neglected. In this case the discharge current

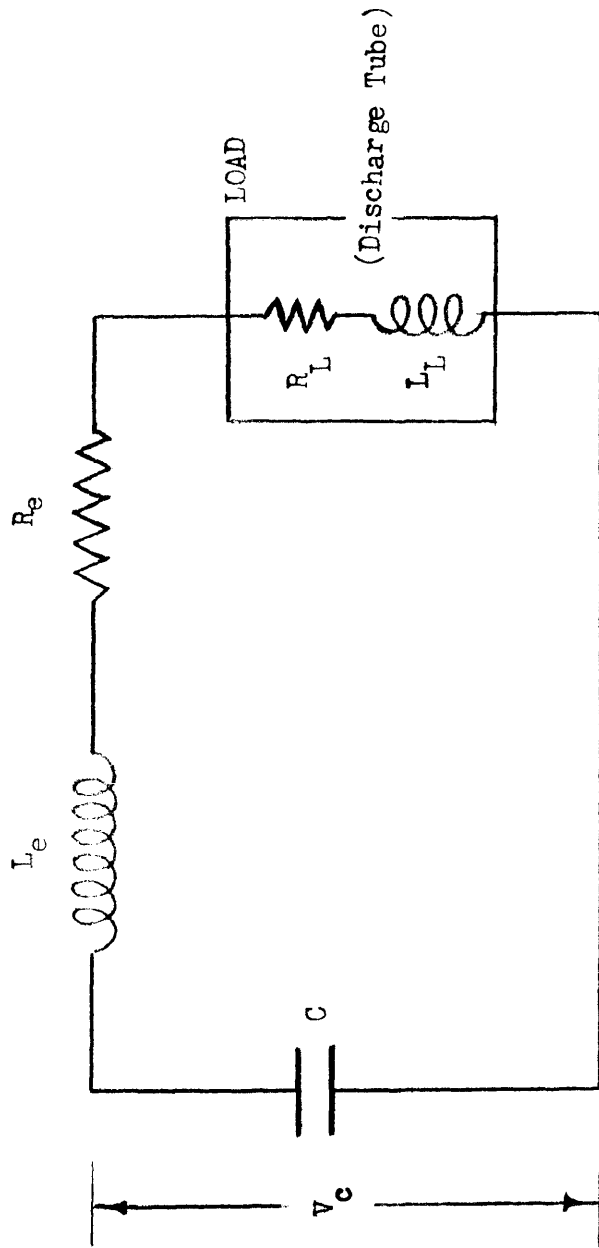


Figure 6.- Equivalent circuit.

is given by:

$$i = \frac{V_c}{\eta L} e^{-\frac{R}{2L}t} \sin \eta t$$

where

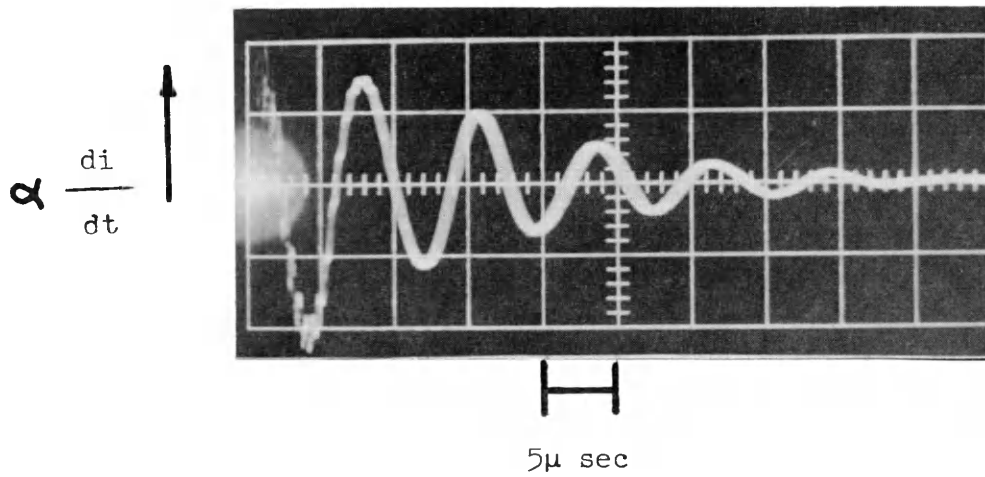
$$\eta = \sqrt{\frac{1}{LC} - \left(\frac{R}{2L}\right)^2} = \frac{2\pi}{T}$$

and R and L are the effective resistance and inductance; T is the period of the discharge. A typical trace of the voltage output from a 1/4-inch-diameter two-turn field coil is displayed on figure 7. This is a time history of the induced voltage across the terminals of the coil. This potential is derived from the time-dependent magnetic flux passing through the coil. Since the magnetic field varies linearly with the current, then the scope trace is proportional to the time derivative of the current. Differentiating the expression above for the current:

$$\frac{di}{dt} = \frac{V_c}{L} e^{-\frac{R}{2L}t} \left(\cos \eta t - \frac{R}{2L\eta} \sin \eta t \right)$$

The effect of the last term is small and is neglected. By measuring the period T and decay factor $R/2L$ of the peaks of the trace the effective resistance and inductance are determined. The results of this calculation for two of the electrode configurations are shown on the figure for the maximum and minimum total energy operating conditions. The peak current

at the first quarter cycle is estimated from $i_{\max} = \frac{2\pi V_c C}{T}$.

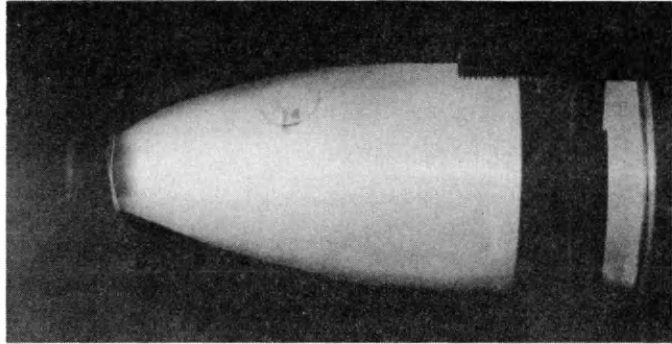


| | Ring-button | Pinch tube |
|--------------------------------|-------------|------------|
| Charging volts, KV | 12.5 | 20. |
| Capacitance, μf | 6 | 9 |
| Period, $\mu\text{ sec}$ | 6.6 | 7.5 |
| Eff. inductance, μh | 0.18 | 0.16 |
| Eff. resistance, ohms | 0.03 | 0.03 |
| Peak current, amps | 72,000 | 127,000 |

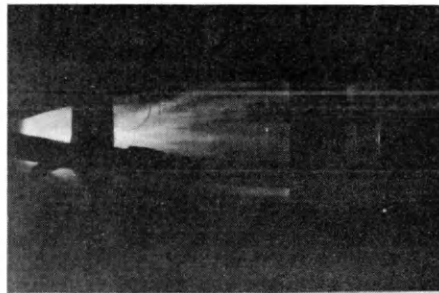
Figure 7.- Typical scope trace of voltage output from field coil and calculated circuit parameters.

C. Pinched Discharge

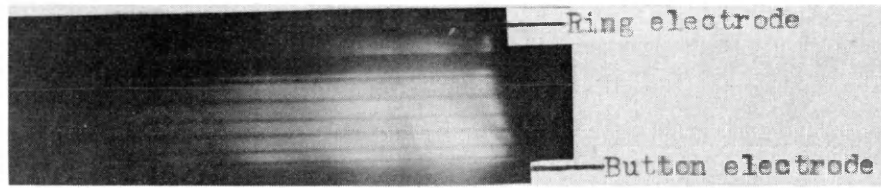
The pinched discharge was examined qualitatively with the smear camera, time-average photographs, and the Kerr cell. The results are summarized in figure 8. The time-average photograph shows a region of high luminous intensity localized in a small column along the tube axis. The width of the column is greater near the button electrode and seems to taper to a narrow pencil ray of hot gas at the exit of the shock generator. Details of the discharge are shown in the Kerr cell picture. In the region of button electrode a highly luminous "ball" is evident. Distinct luminous rays emanate from this "ball" and proceed to the ring electrode apparently along the inside wall of the conical glass section. The hot pencil ray in the center of the tube is not evident. The streak camera smear was obtained by placing a 1/2-inch slit along the glass cone and placing distance markers an inch apart perpendicular to the tube axis. It shows that the illumination first begins at the button electrode and progresses toward the ring electrode. Before passing through the ring electrode the luminous-front speed is greatly increased. The existence of a second luminous wave beginning at the same time as the first wave at the button electrode can be seen. From these data a model of the discharge is constructed. When the discharge is first initiated the ionized gas is immediately forced to the center of the tube by the self-induced magnetic field which, because of the axial nature of the discharge, is perpendicular to the tube axis. This pinching takes place at the button electrode first because of the large current density in this region. The temperature and pressure of the gas are rapidly increased and as the conducting fluid tries to expand it is pinched more into the tube axis. This traveling



(a) Time average photograph.



(b) Kerr cell, $1/10\mu$ sec exposure.



(c) Streak camera smear.

Figure 8.- Characteristics of pinch discharge.

pinch drives the hot gas out of the ring electrode where it expands and forms a strong luminous shock front. Because the expansion takes place both along the axis and the tube radius the shocks would be expected to have a curved contour. This is indeed the case and will be discussed in a later section. It is noted that these results are consistent with the description of the pinch given by Josephson and Hales (ref. 16) for the same type of shock tube. Their test gas was deuterium and the ringing frequency was 210 KC with a maximum current of $\sim 2 \times 10^5$ amps. They observed only one pinch followed by a second sheath of hot gas with an image converter camera. Their scope traces of the potential at the button electrode, however, indicated as many as three successive pinches. Although the smear pictures in this investigation only resolved one pinch and a second luminous front they did indicate (more clearly on the negatives) that the total light intensity in the discharge tube tended to oscillate with the period of the discharge. This would indicate several heating cycles. Josephson and Hales also pointed out that the secondary wave eventually caught up with the primary wave downstream and reinforced the leading front. This was observed in this investigation and is discussed later.

D. Performance of Shock Generators

The rotating mirror camera was used to obtain the primary luminous-front velocities. Slits were placed along the axis of the shock tube and black pieces of tape were used as distance markers (in the streaks presented these markers are 1 inch apart). The luminosity smear exhibits the shock front as a curve of distance versus time on the

35-mm strip film. A counter supplied with the camera accurately measures the speed of the rotating mirror. The velocity of the luminous front is then proportional to the slope of the curvature of the light smear. Experimentally the tangent of the angle at a point on the smear front was measured and the velocity computed from:

$$U_s = C \cdot \text{RPS} \cdot \tan \theta$$

The constant C was determined from the geometry of the camera and the magnification factor of the optics; RPS is the speed of the mirror in revolutions per second, and θ is the measured angle.

Figures 9, 10, and 11 show the primary luminous-front velocity as a function of the initial shock-tube pressure for constant distance from the exit of the shock generator for the three electrode configurations. The performance of the ring-button configuration at 12.5 KV and 6 μf is shown on the first figure. At distances near the ring electrode velocities are higher for the higher pressures. Farther downstream the velocity begins to be inversely proportional to the initial tube pressure. The waves exhibit more attenuation at the higher pressures. Apparently better energy transfer to the gas is accomplished at the higher pressures. The same trends are shown on the next figure for the spindle-cone configuration. The poor performance of this generator is attributed to energy trapped in the cone by reflecting shocks off the inside walls. The lines drawn through the experimental points indicate only the general behavior of the primary shock velocity. The curves are complicated at some distance from the exit of the shock generator by the reinforcement of the primary shock by secondary waves. In both these

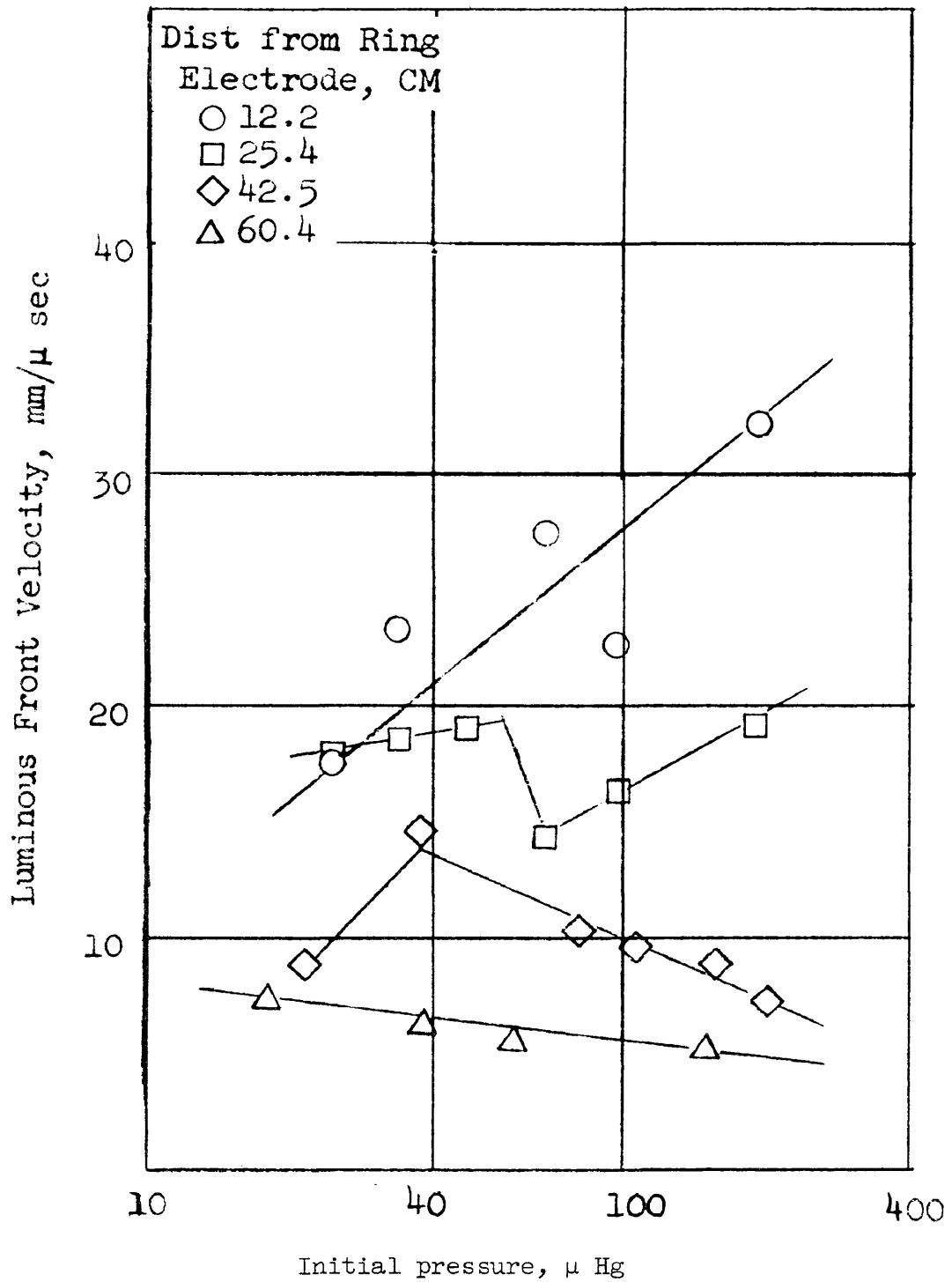


Figure 9.- Luminous front velocity as a function of initial pressure for button-ring configuration at 12.5 KV and 6μf.

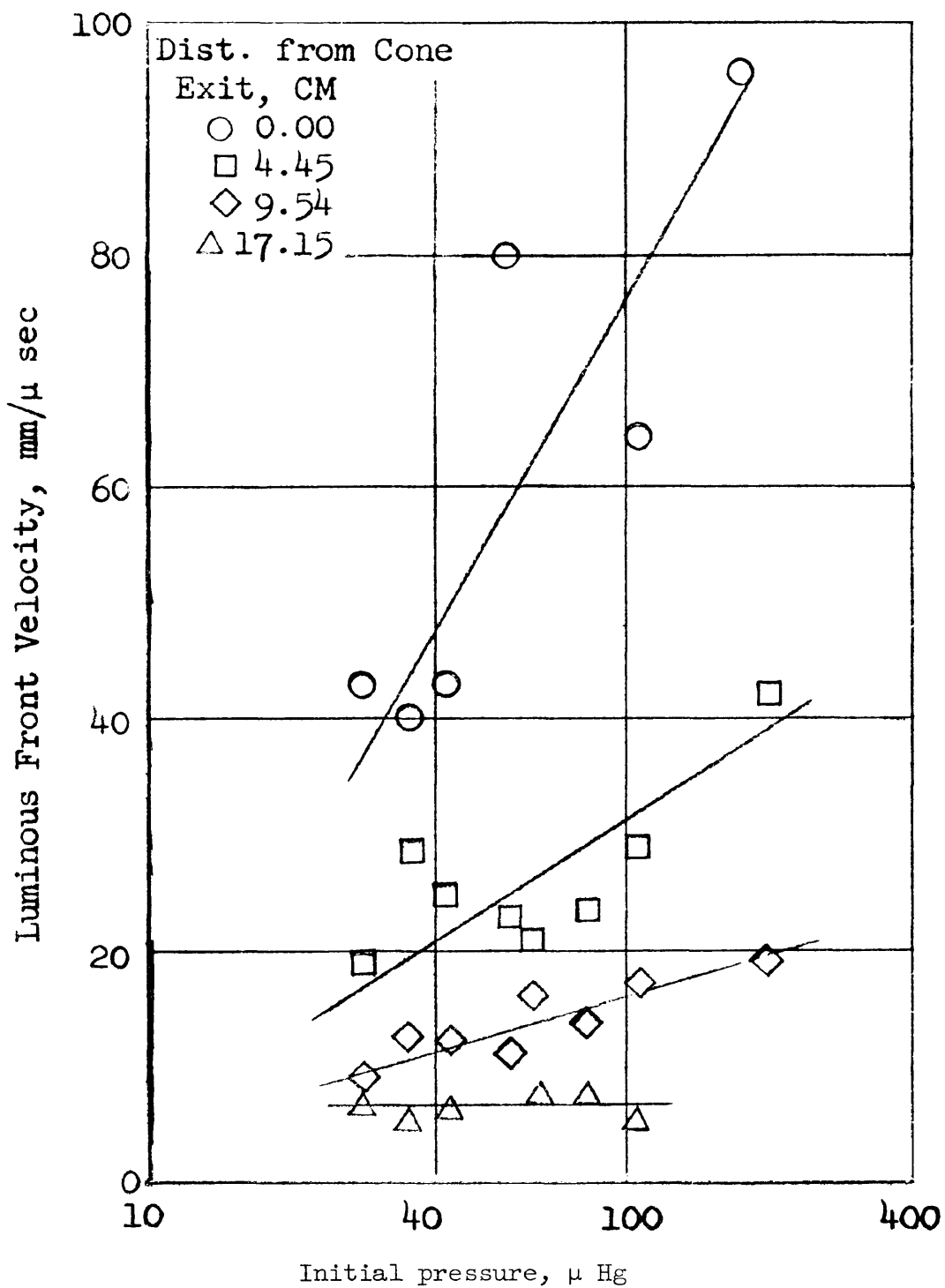


Figure 10.- Luminous front velocity as a function of initial pressure for spindle-cone configuration at 15 KV and 6μf.

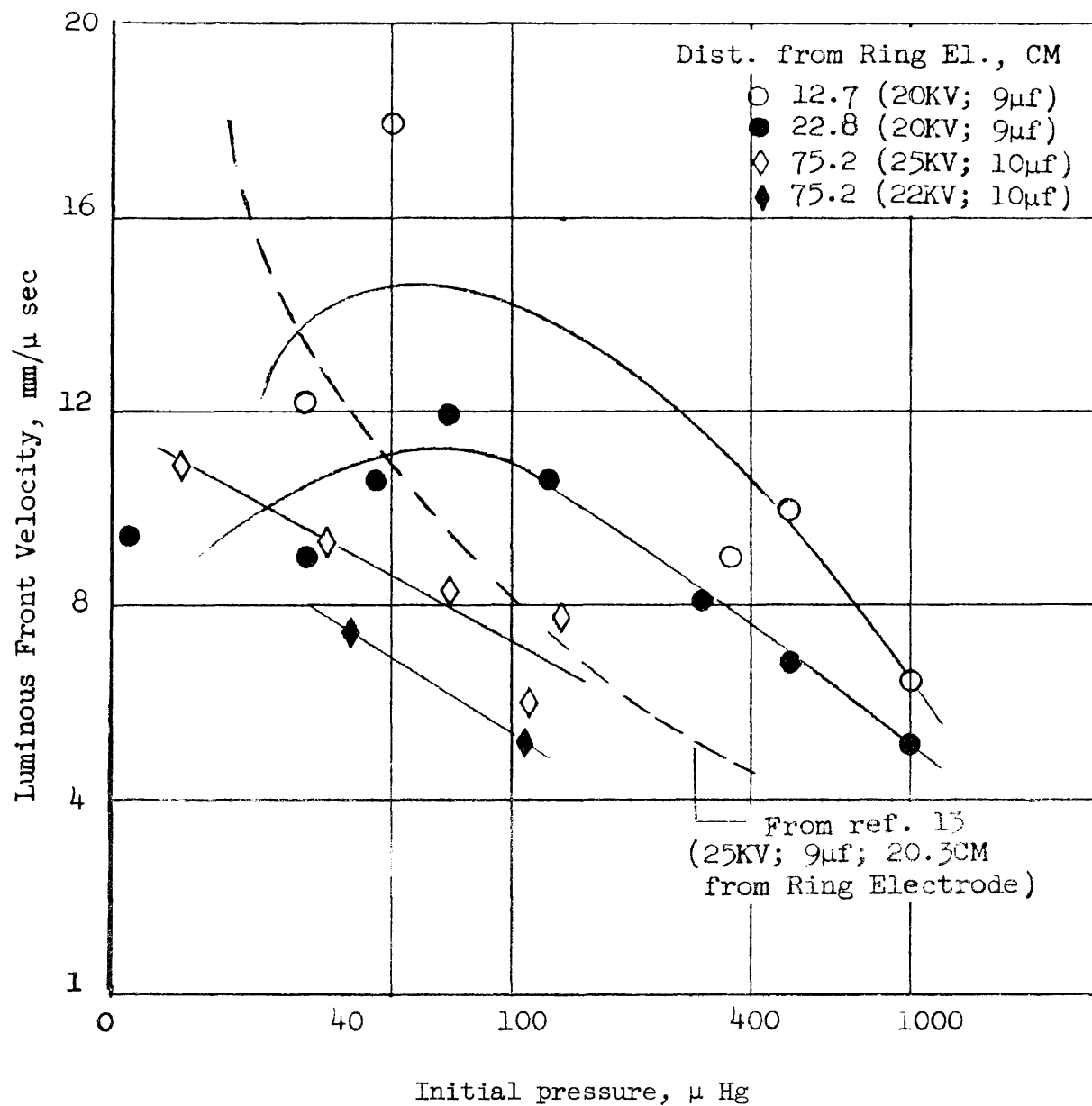


Figure 11.- Luminous front velocity as a function of initial pressure for the pinch tube configuration.

generators secondary waves were apparent at every half cycle of the ringing discharge. This is shown for the ring-button configuration on figure 12 in which twice the time interval of appearance of the multiple waves is correlated to the period of the ringing discharge.

Figure 11 shows the performance of the pinch tube under several initial voltage conditions. The dashed line represents the operational curve of Ziemer's tapered tube as taken from reference 13 for 25 KV and 9 μ f in air at a distance of 20.3 cm from the ring electrode. A comparison of the curves indicates the performance of the pinch tube follows closely that of Ziemer's apparatus.

Typical smear records are shown on figure 13 for the three generators. They indicate the attenuation of the primary wave and also the production of multiple fronts and their interactions. These fronts are particularly numerous in the case of the first two configurations, and as was pointed out, their appearance corresponds closely with the period of the discharge. However, in the case of the pinch tube only three secondary fronts are noted. One follows very closely behind the primary front and the other two at farther distances. Smears farther downstream confirm the intersection of these secondary fronts with the primary wave thus enhancing its speed.

The attenuation of the waves is seen in figure 14 for the pinch tube at two different pressures, and figure 15 shows the attenuation for the other two configurations. It also illustrates the interaction and reinforcement by a secondary wave. The attenuation based on strong one-dimensional blast-wave theory (ref. 17) is inversely proportional to the

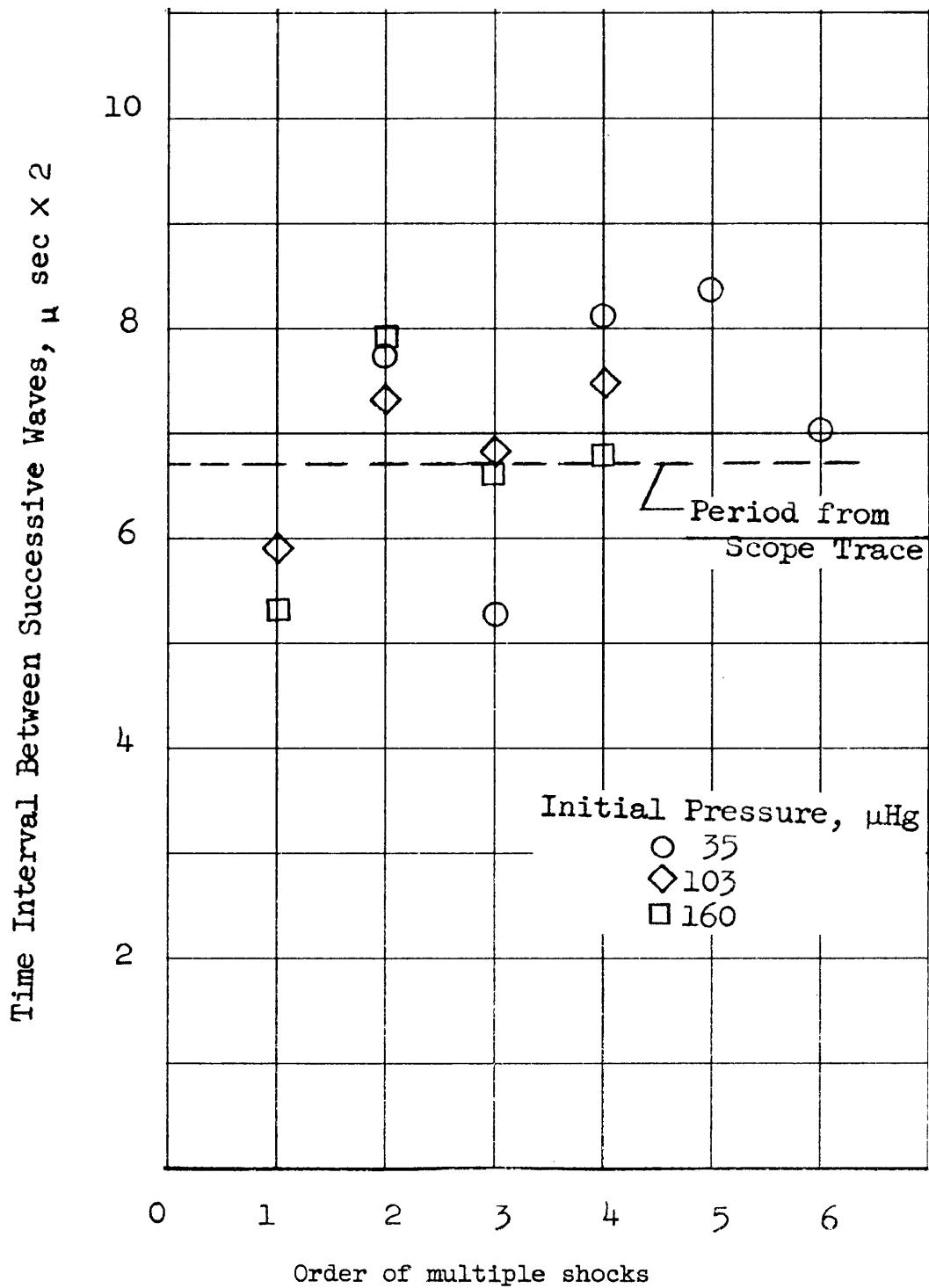


Figure 12.- Time separation of secondary waves generated by button-ring configuration at a distance of 17.8 CM from ring electrode (17.5 KV; 6 μ f).



25 μ Hg

(a) Button-ring configuration (17.5 KV; 6 μ f).

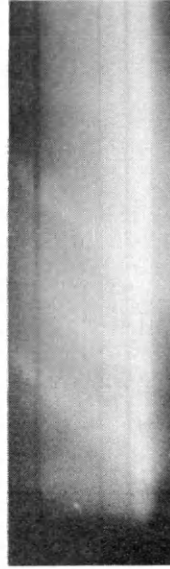


160 μ Hg



35 μ Hg

(b) Spindle-cone configuration (15 KV; 6 μ f).



10 μ Hg

(c) Pinch tube (20 KV; 9 μ f).

Figure 13.- Typical velocity smears showing luminous front attenuation and multiple shock interaction.

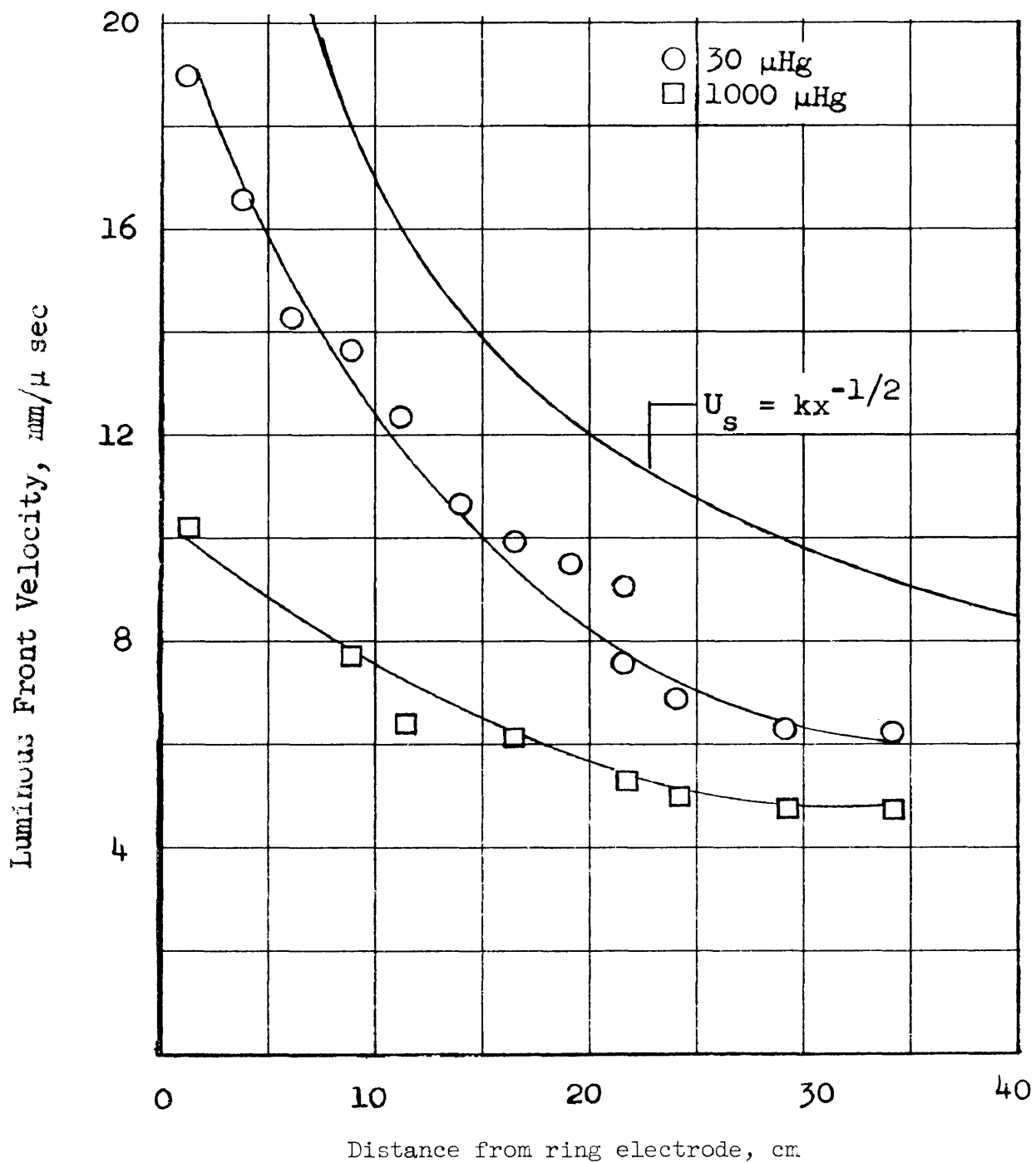


Figure 14.- Attenuation of luminous front generated by pinch tube configuration at 20 KV and 9μf.

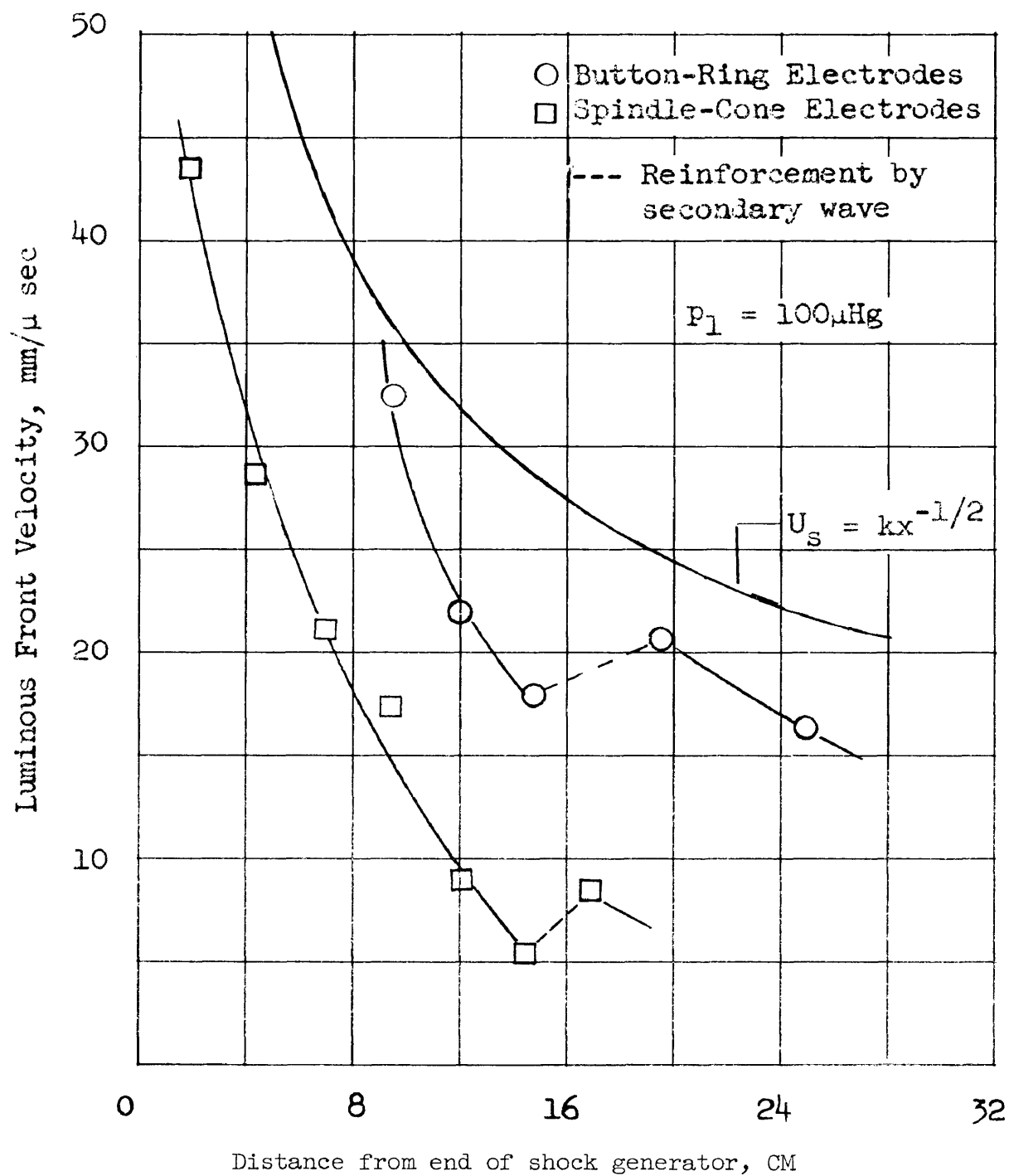
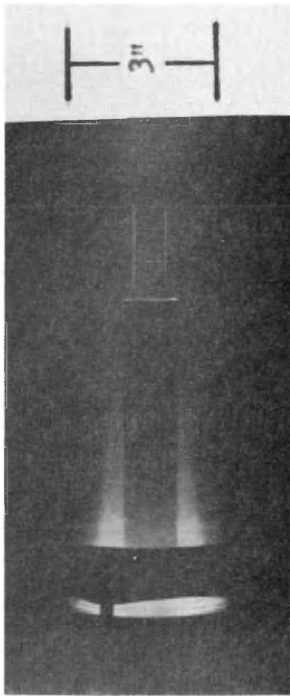


Figure 15.- Interaction of primary luminous front and secondary wave at 15 KV and 6μf.

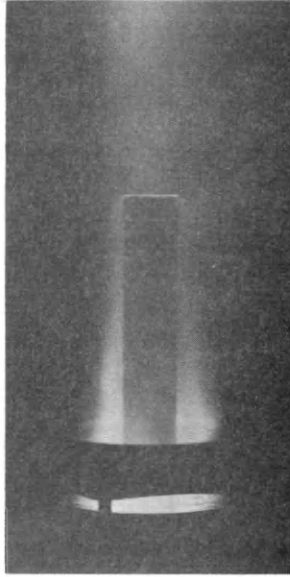
square root of the distance from the blast.¹ This decay law is plotted on each of the curves. In the case of the pinch-tube shocks the agreement is fair, but the other configurations indicate stronger attenuation. This is certainly to be expected in the case of the spindle-cone configuration since the diameter of the exit of the hot gas from the electrode is small. Thus, the expansion of the gas in the radial direction would decrease the luminous front speed in the axial direction.

If models are placed in the flow of the primary wave strong luminous gas caps are observed. Figure 16 shows the results of time-average photographs of the bow waves. These pictures were obtained with a Graphax camera with a polaroid film attachment. A pair of crossed plane polaroids were used to obtain contrast between the illumination from the free-stream gas and hot gas cap wave. The duration of this standoff wave was measured with the streak camera for a pressure of 10 μ Hg. The steady wave duration was about 15 microseconds. Ziemer (ref. 11) made a survey

¹For a strong one-dimensional blast wave the internal energy per unit volume is $E = \frac{1}{2} \rho u^2$, where ρ is the gas density behind the wave and u is the gas velocity. If the expansion is pictured as having constant energy, and a weak dependence of ρ on distance is assumed, then the total energy of the system is: $W = \int_0^x \left(E + \frac{1}{2} \rho u^2 \right) d\tau$, where $d\tau$ is the one-dimensional volume element. Substituting for E and removing ρ from under the integral we find, $W \sim \rho u^2 x \sim \rho U_g^2 x$, where U_g is the shock front velocity. Therefore the attenuation is given by: $U_g \sim x^{-1/2}$.



$P_0 = 25\mu \text{ Hg}$



$P_0 = 350\mu \text{ Hg}$

Model: Hollow steel tube



$P_0 = 375\mu \text{ Hg}$

Model: Bolt head

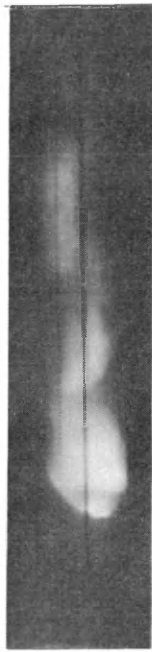
Figure 16.- Time-average photographs of luminous bow waves.

of these flow durations in air for varying initial tube pressures. He found that the bow wave remained for a longer time at the low-shock-tube pressures and at distances closer to the ring electrode.

A comparison of the three generators shows that the primary wave of the pinch-tube configuration exhibits less attenuation and fewer multiple-shock interactions. Since the shock flow appeared to be less complicated, the pinch-tube generator was the only one considered in the following discussion of shock profile, reflected waves, and time-integrated spectra.

E. Shock Profile

The shock profiles were obtained with the streak camera by placing observation slits perpendicular to the tube axis. If the shocks are curved then points in the slit will be illuminated at different apparent times relative to the moving film as the luminous front passes by the slit. Since the writing speed of the camera in all cases is slower than the luminous-front velocity, the actual profiles are more parabolic than indicated. Figure 17 presents typical shock-profile smears obtained with the pinch tube at the exit of the ring electrode and at some distance downstream of the discharge. These pictures indicate that the shock is parabolic and does not flatten much with distance. The trailing lumina-tion does not appear to be uniform, thus implying a turbulent gas motion. Fowler and Turner (ref. 18) were able to alter greatly the profile of electromagnetically driven shocks by the application of strong axially magnetic fields up to 20,000 gauss. Their shocks were generated in a 1-inch-diameter tube in deuterium. At zero fields the shocks showed a bulge in the center as in this investigation. The application of the

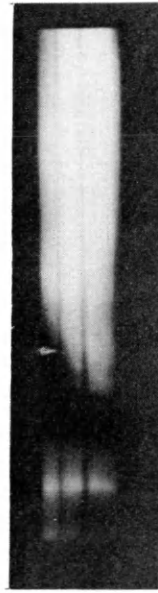


500 μ Hg

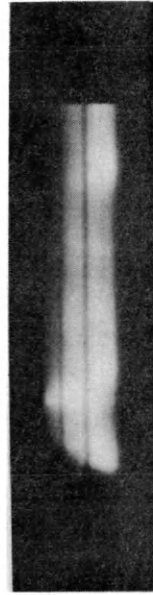


28 μ Hg

(a) At exit of ring electrode.



500 μ Hg



29 μ Hg

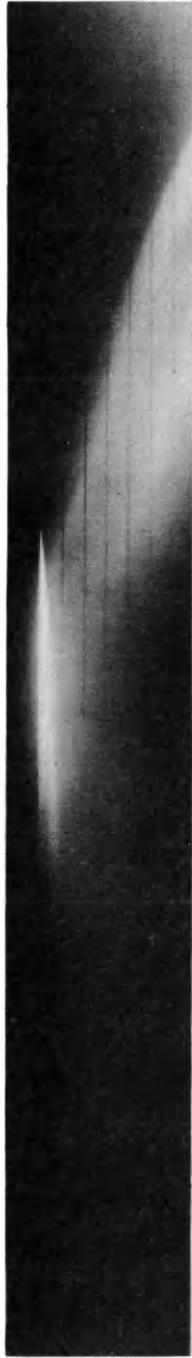
(b) At 17.8 CM from ring electrode.

Figure 17.- Profile of shocks generated by pinch tube (20 KV; 9 μ f).

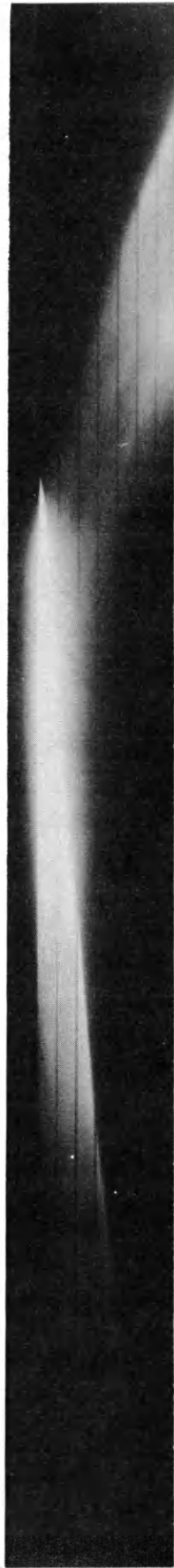
axial field made this bulge more pronounced. With zero field the parabolic contour is explained by assuming that the gas along the axis is hotter than near the wall.

F. Reflected Luminous Fronts

A brass plug $2\frac{3}{4}$ inches in diameter was placed in the shock tube at three different positions from the ring electrode in the pinch-tube generator. Smears were obtained of the primary wave and the reflecting wave off the plug through a half-inch slit along the tube axis. Figure 18 shows typical pictures of the reflection process for the plug at a distance of 35.6 cm from the ring electrode. Time-average photographs of the hot gas reflecting off the plug at three different pressures are shown in figure 19. A definite curved pattern of the hot gas standing in front of the plug is evident. From the smears it is observed that as the reflected wave propagates into the stream of the oncoming wave it is generally retarded at about 2.5 cm from the plug. The wave then regains speed and advances with increasing velocity up the shock tube. Another important feature is that the luminosity from the reflected wave appears to begin at the plug before the primary wave reaches the end of the shock tube. This is especially evident at the higher pressures. At times a faint luminous wave can be detected ahead of the intense luminous primary wave and it appears to coincide with the beginning of the reflected wave luminosity at the reflecting wall. This indicates a relaxation process taking place behind the incident wave. Since the radiation is mainly electronic in nature, the extent of the relaxation zone is interpreted as a rough measure of ionization relaxation behind strong shocks in air.



35 μ Hg

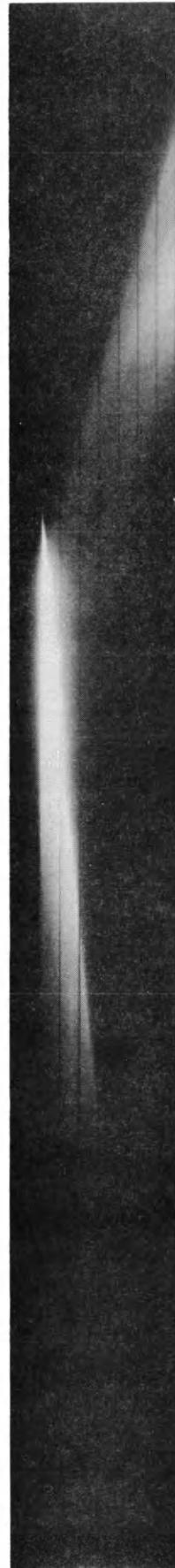


60 μ Hg

|— 12 μ sec —|

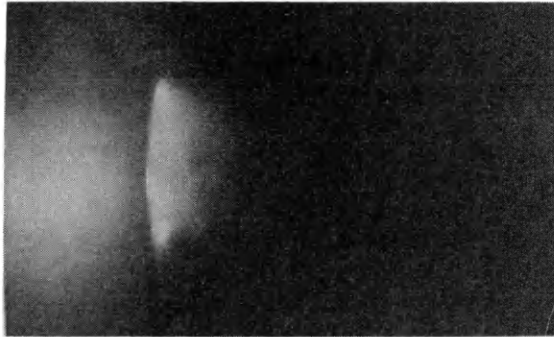


500 μ Hg

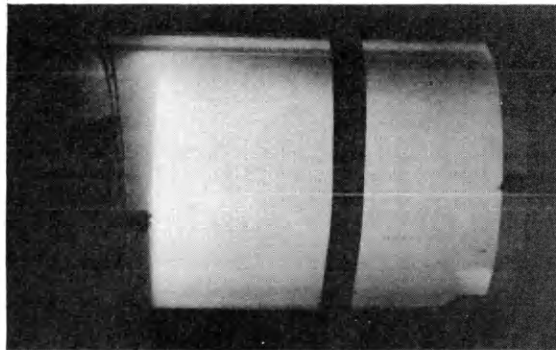


1,000 μ Hg

Figure 18.- Velocity smears of reflection off brass plug at 35.6 CM from ring electrode of pinch tube (20 KV; 9 μ f).



$$p_0 = 12\mu \text{ Hg}$$



$$p_0 = 124\mu \text{ Hg}$$

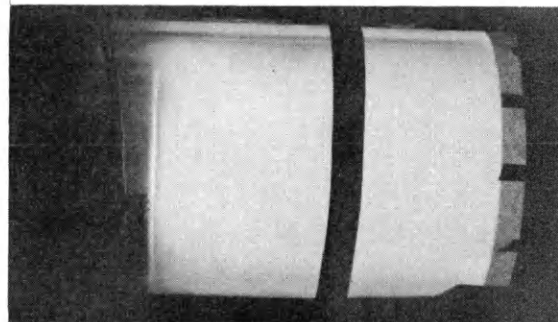


Figure 19.- Time-average photographs of hot gas reflecting off brass plug located 9 inches from ring electrode.

Niblett and Blackman (ref. 19), for example, have used this property of the reflection of strong luminous shocks to obtain an approximate measure of ionization relaxation in air.

The reflected wave velocities were compared to an average incident shock velocity. This average shock velocity was calculated by measuring the time for the luminous front to travel from the exit of the shock generator to the reflecting plug. The incident velocity at the plug was also measured but was not felt to be a good indication of the energy of the oncoming flow because of interactions with multiple shocks which at times gave a relatively high shock velocity at the plug. In all cases the average shock velocity was less than the velocity measured at the reflecting plug. Figure 20 shows a plot of the ratio of the measured reflected velocity at the plug to the average oncoming flow velocity as a function of the average velocity. Assuming that this average velocity corresponds to the effective incident velocity at the plug, the expected reflected ratio based on equilibrium flow considerations behind an incident normal shock in real air (ref. 20) (that is, taking into account dissociation and ionization in equilibrium) is shown in the dotted area. This area represents a series of curves covering the pressure range considered in this experiment. The measured reflected ratios show a general trend to deviate from the equilibrium theory as the strength of the incident wave decreases. Within the experimental accuracy of making the velocity measurements, roughly 25 percent, the reflected ratios are on the average at least a factor of 2 greater than the predicted values. The average effect of the initial shock-tube pressure on the reflected ratio is shown in figure 21. The line drawn through

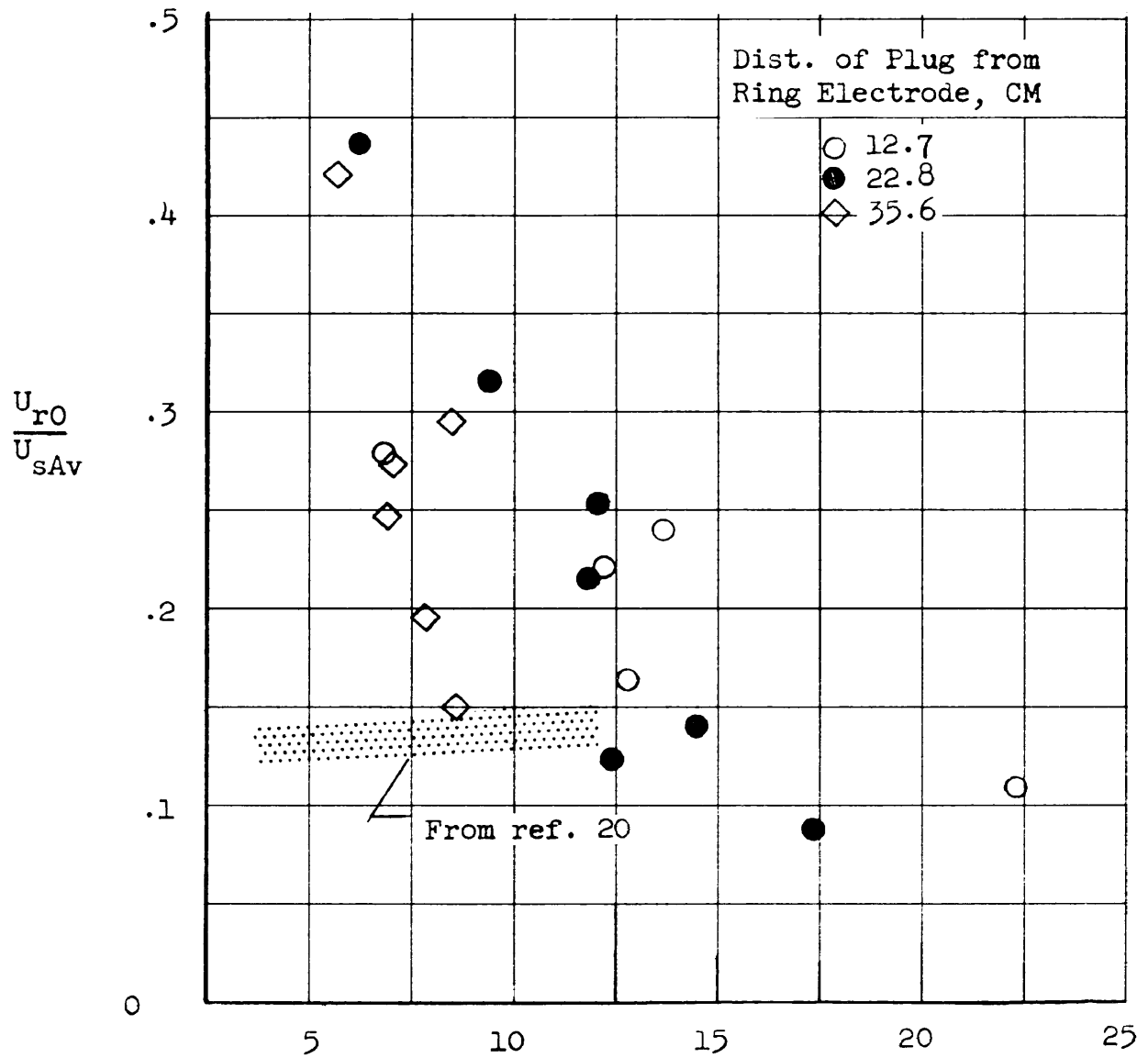


Figure 20.- Average effect of incident shock velocity on reflected shock velocity at plug.

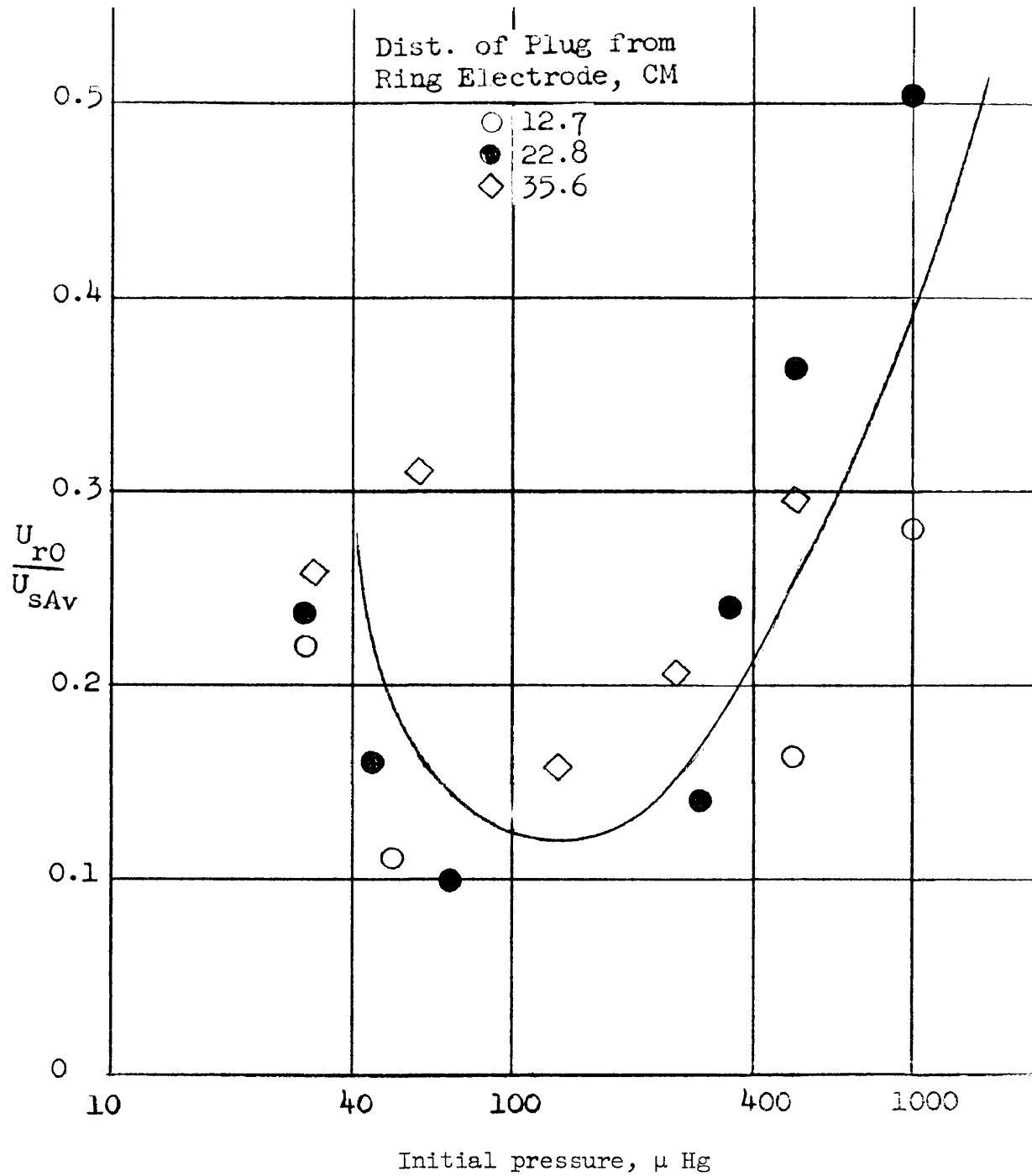


Figure 21.- Average effect of initial pressure on ratio of reflected shock velocity at plug to average incident shock velocity.

the points is an "eyeball" estimate of the trend of the points. This curve shows that the ratios which deviated most from the equilibrium theory occur at the higher pressures. Figure 22 is a plot of the reflected velocity ratio measured at 10.2 cm upstream of the plug as a function of the average incident velocity. It is evident from this curve that the reflected velocity upstream is greater than the reflected velocity at the plug. The reflected waves are discussed further in the summary.

G. Time-Integrated Spectra

Spectra were obtained in three different regions of the shock tube. An acrylic, 1/8-inch-thick, window was placed at the end of the shock and the discharge was observed by placing the spectrograph slit next to the window without any focusing optics. Spectra were also obtained looking perpendicular to the tube downstream of the ring electrode and looking directly at the pinch discharge tube without focusing optics. Samples of the spectra are displayed on figure 23. The spectrum looking up the tube axis exhibits a background continuum; the spectra are electronic in nature and no band structure is evident. Most of the lines were identified using the MIT wavelength tables (ref. 21) and the spectrum was found to be characteristic of spark spectra in air as taken from reference 22. The lines were identified to within $\pm 0.5 \text{ \AA}$. The OI and OII lines are especially sharp while the nitrogen lines are less numerous and often seem hazy and broad. The CaII lines at 3933.7 \AA and 3968.5 \AA and the AlI lines at 3944.0 \AA and 3961.6 \AA were present in all the spectra as well as strong SiI lines at 3905.5 \AA and $4128.1-30.9 \text{ \AA}$. Some

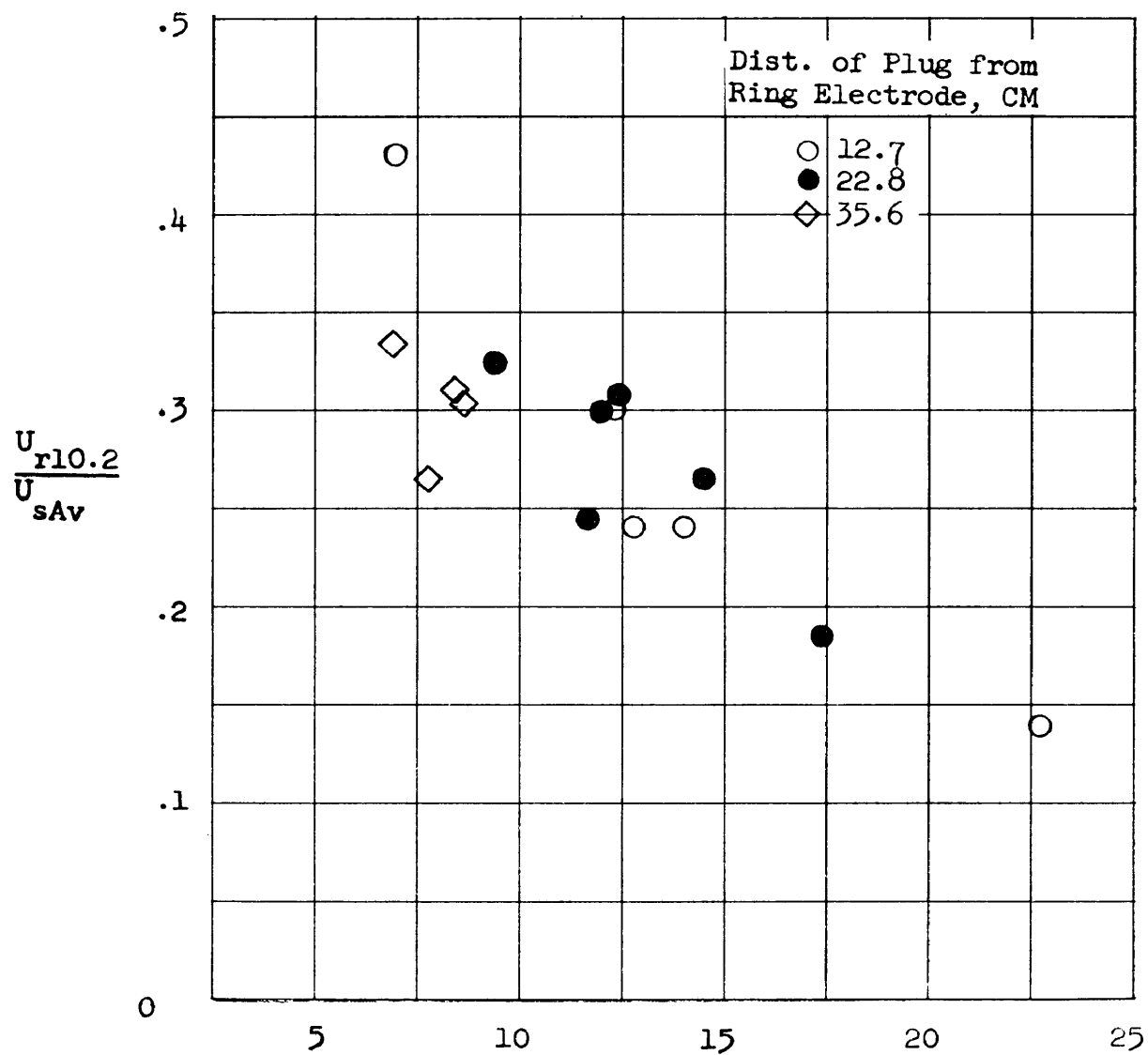
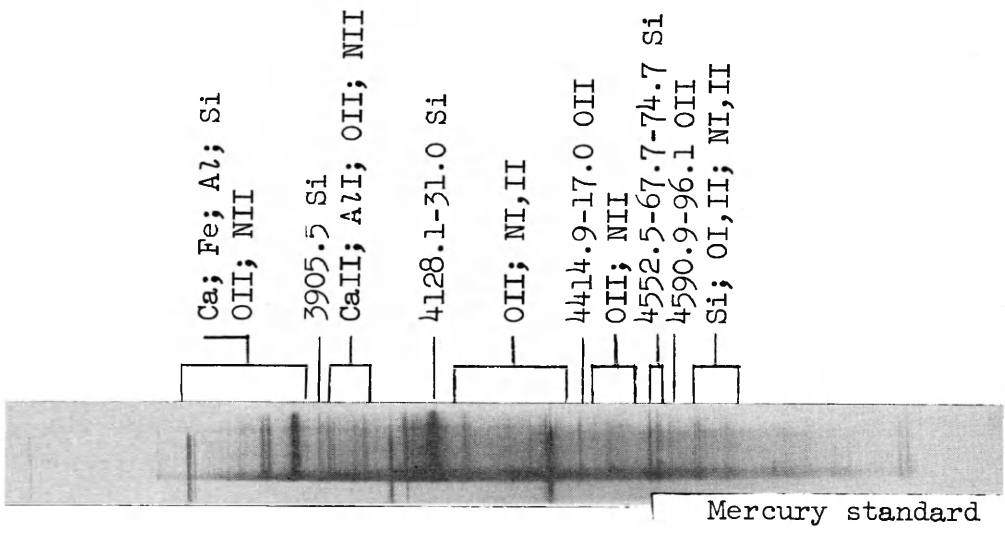


Figure 22.- Average effect of incident shock velocity on reflected shock velocity at 10.2 CM from plug.



(a) Looking down tube axis.



(b) Looking perpendicular to pinch tube.



(c) Looking perpendicular to shock tube downstream of discharge.

Figure 23.- Time-integrated spectra of discharge from pinch tube.

weak iron and CuII lines were observed. The absence of more numerous and stronger copper lines is puzzling since the electrodes were copper and the button electrode did show some erosion. No lines were detected in spectra (b) and (c) which were not identified in the spectrum (a) looking up the tube axis. In order to see lines looking downstream of the discharge, the spectrograph slit was opened wider. The strong lines observed are from CaII, AlI, and SiI. Faint lines on the negative exhibit sharp lines of OI and OII. The spectrum in figure 24 of the air gap switch discharge offers an interesting contrast to the low-pressure air discharge. Again the CaII and AlI lines were present. The iron and silicon lines are attributed to the brass trigger and insulator. The major portion of the spectrum is due to copper, CuI and CuII. No oxygen or nitrogen lines are present.

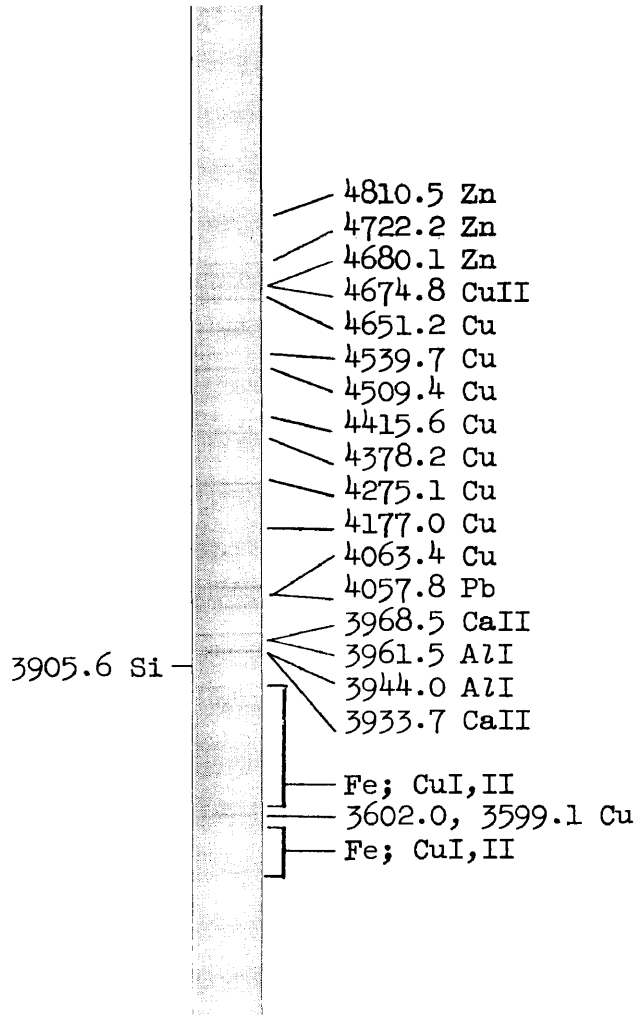


Figure 24.- Time-integrated spectrum of air gap switch discharge.

CHAPTER III

SUMMARY AND CONCLUDING REMARKS

Shock Mach numbers of $M_s \sim 150$ were obtained at the exit of the generators. The shock wave was strongly attenuated and decayed to $M_s \sim 20$ downstream approximately 6 inches from the ring electrode. Because of the ringing of the electrical discharge, multiple shocks were generated at each half cycle. In the case of the pinch tube these secondary waves were not as numerous and the shock flow was more uniform. The shock profiles indicated a parabolic contour and nonuniformity of the intensity of the illumination behind the primary wave. The waves did not flatten as much as they propagated. Steady flow times (time interval of a constant luminous standoff distance on a blunt model) were on the order of tens of microseconds. The behavior of the pinch tube was found to be in agreement with the experience of others.

The reflected waves were found within the experimental error, roughly 25 percent, to exhibit velocities consistently greater than those predicted by equilibrium shock theory. On the basis of an ideal shock tube for strong shocks the limiting reflected ratio is given by:

$$\frac{U_{ro}}{U_s} \approx \frac{2(\gamma - 1)}{(\gamma + 1)}$$

where γ is the specific heat ratio. For air with $\gamma = 1.4$ this value is one-third so that the ratios lie between one for sound waves and

one-third for strong shock waves. If a real gas is considered, the specific heat ratio will decrease below one-third as dissociation and ionization of the gas sets in. This reflects the increase in the number of degrees of freedom of the system as rotational, vibrational, and eventually ionization energy modes are excited. The effect on the shock velocity ratio, for the range incident shock velocities encountered in this work, is to decrease it to values less than 0.18. In attempting to explain this difference it should be pointed out that the shock waves generated in the electromagnetic shock tube are more analogous to blast waves. Such waves propagate with a decaying pressure behind the wave as in contrast to the slug of uniform gas assumed behind the moving normal shock. The fact that the reflected velocity increased in speed as it propagates farther upstream suggests that the wave is traveling head on into the rarefaction wave which is reflected from the discharge region. On the basis of elementary theory the head-on collision of a shock wave and a rarefaction wave could give rise to an enhanced shock velocity. Looking again for analogies with the ideal shock tube, the fact that the reflected wave was initially retarded and in some cases turned around and started all over again at the reflecting plug seems to suggest the interaction of a head-on collision of a shock wave and a contact surface. In this case ideal theory predicts a retardation of the shock. However, in the case of the reflected velocity ratio at the wall a more complex explanation seems necessary. The high value of the reflected velocities would seem to indicate, based on the equation above, a reduction in the effective degrees of freedom of the system and

thus a larger specific heat ratio. It would appear that certain non-equilibrium processes and three-dimensional effects must be considered in order to explain the large reflected velocities measured in this investigation.

The time-integrated spectra of the low-pressure discharge were characteristic of spark spectra in air. Strong line radiation from silicon indicated contamination from the glass walls; although the electrodes showed some erosion, only faint copper lines were evident. In the main, the spectrum viewing along the tube axis or directly at the glass discharge region was characterized by sharp line radiation from neutral and singly ionized oxygen; nitrogen lines were often hazy and diffuse. It is not apparent from such time-integrated spectra how severely the contamination level would affect radiation heating studies on a blunt obstacle placed in the shock flow.

In conclusion, the electromagnetic shock tube is an attractive device for producing very strong shocks for short durations. However, it has been shown that the luminous shocks are far from simple. The flow exhibits nonuniform gas properties and seems to be pictured more as a turbulent "ball" of gas with no definite contact surface interface. Reflection of this "ball" of gas was complex and the reflected velocities were greater than predicted on the basis of equilibrium theory. A consideration of nonequilibrium thermodynamics seems necessary to explain certain aspects of the electromagnetically driven shock tube. In view of these facts, it is concluded that the use of the flow generated

in the laboratory. The data described in this report for studies
in hypobaric chambers, and the effects of radiant heating,
to a certain extent, must be approached with reservation.

REFERENCES

1. Wright, J. K.: Shock Tubes, Methuen Monograph, New York: John Wiley & Sons, Inc., 1961.
2. Glass, I. I. and Hall, J. G.: Handbook of Supersonic Aerodynamics, Section 18, Shock Tubes, Navord Report 14488, vol. 6, December 1959.
3. Bloxom, D. E., Jr.: Electrically Driven Shock Tubes, J. Appl. Phys., vol. 29, July 1958, p. 1128.
4. Nerem, R. M. and Lee, J. D.: Initial Performance of the Ohio State University Arc Discharge Shock Tube Facility, Proceedings of Supersonic Tunnel Association, vol. III, April 26-27, 1962.
5. Bethe, Hans A., et al.: Blast Waves, Los Alamos Scientific Laboratory, Los Alamos, New Mexico, LA-200, March 27, 1958.
6. Fowler, R. G. and Lee, R. J.: Rayleigh Afterglow in Hydrogen Discharges, Phy. Rev., vol. 81, Jan.-Mar. 1951, p. 457.
7. Fowler, R. G., Goldstein, J. S., and Clolfelter, B. E.: Luminous Fronts in Pulsed Gas Discharges, Phy. Rev., vol. 82, no. 6, June 15, 1951, p. 879.
8. Fowler, R. G., Atkinson, W. R., Compton, W. D., and Lee, R. J.: Shock Waves in Low Pressure Spark Discharge, Phy. Rev., vol. 88, 1952, p. 157.
9. Kolb, A. C.: Experiments at U.S. Naval Research Laboratory, Magneto-hydrodynamics, edited by R. Landshoff, Standard University Press, Standford, California, 1957, p. 76-91.

10. Kash, S. W.: Experiments at Lockheed Missile Systems Division, Magnetohydrodynamics, edited by R. Landshoff, Standford University Press, Standford, California, 1957, pp. 92-98.
11. Josephson, V.: Production of High Velocity Shocks, J. of Appl. Phy., vol. 24, no. 1, January 1958, pp. 30-32.
12. Ziemer, R. W.: Electromagnetic Shock Tubes, Dynamics of Conducting Gases, Proceedings of the Third Biennial Gas Dynamics Symposium, Editors, Cambel, A. B. and Fenn, J. B., Northwestern University Press, Evanston, Ill., 1960, pp. 139-149.
13. Ziemer, R. W.: Experimental Investigation in Magneto-Aerodynamics, ARS Journal, vol. 29, no. 9, September, 1959, p. 642.
14. Ziemer, R. W.: Instrumentation for Magnetoaerodynamic Heat Transfer, Space Technology Laboratories, Inc., STL/TR-60-0000-09290, September 8, 1960.
15. Cobine, J. D.: Gaseous Conductors, Dover Publications, Inc., New York, 1958, pp. 177-181.
16. Josephson, V. and Hales, R. W.: The Structure of an Electromagnetically Driven Shock Tube, Space Technology Laboratories, Inc., STL/TR-60-0000-09093, April 14, 1960.
17. Harris, E. G.: Exact and Approximate Treatments of the One-Dimensional Blast Wave, NRL Report 4858, Nov. 25, 1959.
18. Fowler, R. G. and Turner, E. B.: A Magnetically Insulated Shock Tube, Space Technology Laboratories, Los Angeles, California, STL/TR-60-0000-09180, 1960.

19. Niblett, B. and Blackman, V. H.: An Approximate Measure of the Ionization Time Behind Shock Waves in Air, J. of Fluid Mech., vol. 4, 1958, p. 191.
20. Ziemer, R. W.: Extended Hypervelocity Gas Dynamic Charts for Equilibrium Air, Space Technology Laboratories, Inc., STL/TR-60-0000-09093, April 14, 1960.
21. MIT Wavelength Tables, Compiled by George R. Harrison, John Wiley & Sons, Inc., New York, 1939.
22. Handbook of Chemistry and Physics, Chemical Rubber Publishing Co., 41st Edition, 1959-1960, p. 2906.

VITA

James Franklin Rosch

Born in Washington, D.C., December 8, 1936. Graduated from Phillips Academy, Andover, Massachusetts in June 1955; B.S.; College of William and Mary, Williamsburg, Virginia, 1959. Elected to Phi Beta Kappa, Alpha of Virginia, December 1958. Presently employed by the National Aeronautics and Space Administration at the Langley Station, Hampton, Virginia.